MODIS
Algorithm Theoretical Basis Document
Bio-Optical Algorithms——Case 1 Waters

Dennis K. Clark

National Oceanic and Atmospheric Administration
National Environmental Satellite Service
Washington, D.C. 20233

Version 1.2

CONTENTS

MODIS
ALGORITHM THEORETICAL BASIS DOCUMENT
BIO-OPTICAL ALGORITHMS—CASE 1 WATERS

Dennis K. Clark

30 Jan, 1997

Introduction

A primary goal of the MODIS Oceans Discipline Group research is to extend our knowledge of the big-optical state with the observations of backscattered energy in the visible region of the electromagnetic spectrum. The radiance received at spacecraft altitudes has been modified principally by solar irradiance scattering and absorption processes associated from the air (Rayleigh scattering), from particles suspended in the air (Mie scattering), ozone (selective absorption), sea surface (sun glint), water molecules and suspended particles in the ocean. The marine optical contribution is referred to as the water leaving spectral radiance of the water denoted by $L_w(\lambda)$, where λ is wavelength, and is the only portion of the total observed radiance which contains any information concerning the concentration of ocean constituents. The Nimbus-7 Coastal Zone Color Scanner (CZCS) instrument (Hovis *et al*, 1980) research demonstrated that the observed spectral radiances could be decomposed and a measurement of one of the major bio-optical constituents, nearsurface concentrations of the photosynthetic pigment chlorophyll *a* plus its associated degradation product phaeopigment *a* , could be quantified with at accuracies and precisions useful to marine biology applications. The in-water algorithm development approach serves as the basis for this MODIS research effort.

The in-water bio-optical relationships and algorithms were empirically derived and optimized for the CZCS sensor. In the case of the CZCS this is considered inherently more difficult because of severely restricted spectral information (only three spectral bands could be used for bio-optics). MODIS (and SeaWiFS) instruments will reduce this and several other constraints which limited the CZCS performance and algorithm implementation.

Basically, this empirical approach is being duplicated for MODIS with the additions of enhanced measurement technology and techniques. With this approach, the limiting accuracy for the retrieval of phytoplankton pigment concentration and other potential parameters, such as chlorophyll *a* and total seston, depends upon the degree to which the concentration of the constituent influences the optical properties of natural waters and in particular the degree to which this influence can be quantified.

Experimental Methods and Techniques

In-Water Radiometry.

The actual optical measurements which were carried out on a typically pre- and post-launch bio-optical station are depicted schematically in Figure 1, in which the spectral radiometer denoted by SR1 measures the downwelling spectral irradiance $E_d(z)$ at a depth z, while SR2 measures the upwelling spectral radiance $L_u(z)$ at depth z and SR3, mounted on the deck of the ship, measures the downwelling sky and sun spectral irradiance $E_i(z)$ when SRI and SR2 are at depth z to compensate for variations in the incident irradiance.

Usually measurements are obtained at three depths. The upwelled spectral radiances are then propagated to the sea surface by first calculating the upwelled spectral radiance attenuation coefficient K_L using

$$K_L(\lambda) = \frac{1}{z_2 - z_1} \ln \frac{L_u(\lambda, z_1)/E_i(\lambda)}{Lu(\lambda, z_2)/E_i(\lambda)} \tag{1}$$

and then accounting for the transmittance loss between the surface and z through

$$L_u(\lambda, 0) = L_u(\lambda, z) e^{k_L(\lambda, z)} \tag{2}$$

Nominally, in Eq. (2), z is one meter. The subsurface upwelled radiances are then transmitted through the sea surface with

$$L_w(\lambda) = \frac{t}{n^2} L_u(\lambda, 0) \tag{3}$$

where t is the radiance transmittance and n is the index of refraction of water. The procedures detailed by Equations (1), (2), and (3) follow Austin (1974,1980) where his value of $t/n^2 = 0.543$ was used for the computations. Finally, the CZCS spectral band characteristics taken from Ball Brothers (1979) were applied to $L_w(\lambda)$ to provide $L_w(443)$, $L_w(520)$, $L_w(550)$, and $L_w(670)$, the CZCS surface spectral radiance. These transformed spectral radiances ($L_w(\lambda)$) would represent the signal available to the CZCS in the absence of the atmosphere, and hence, their relationship to the pigment concentration is an essential step in inverting the satellite ocean color measurements.

Phytoplankton Pigment Analysis Review.

Phytoplankton biomass is usually expressed in terms of chlorophyll *a* concentration because of the ease of making these measurements. There are problems associated with using pigment concentration as a measure of phytoplankton biomass: (1) chlorophyll concentration per cell is species specific, (2) older cells have less pigments, (3) light intensity and spectral quality, as well as nutrients affect pigment composition and concentration, (4) usually only chlorophyll *a* is measured although other pigments are present (chlorophylls *b* & *c*, carotenoids, and phycobilisomes), and (5) chlorophyll concentration and cell size are not always correlated.

There are three recognized methods for measuring phytoplankton pigments: spectrophotometric, fluorometric, and High-Performance Liquid Chromatography (HPLC). The spectrophotometric method (Strickland and Parsons, 1972) is not currently a standard technique because large filtration volumes are required and errors are induced because absorption bands of accessory pigments overlap the chlorophyll *a* bands. The fluorometric method, which also suffers from overlapping absorption bands, was developed by Yentsch and Menzel (1963) and later modified by Holm-Hansen *et al.* (1965) to measure chlorophyll *a* and phaeophytin *a*. This method was used to ground truth CZCS ocean color data, and with procedures then in use, the precision of the method was estimated to be about 30%. Much of this variability was attributed to differences in sampling, filtration, extraction and calibration protocols such as filtration volume, storage time before filtration, vacuum pressure, filter type (e.g. Millipore, GFC, GFF, Nuclepore), type of extraction solvent, extraction method (grinding, sonication, 24 hour), calibration standard (pure chlorophyll *a* , diatom culture), etc.

An example of this variability is shown in Figure 2 which compares the fluorometric determination of chlorophyll *a* measured during the post-launch CZCS validation cruise in the Gulf of Mexico (1978). Drs. C. Yentsch and C. Trees collected samples from the same Niskin bottles, but measured chlorophyll *a* using different protocols. These comparisons are illustrated in Figure 2. From the figure, it is obvious that GFF filters consistently gave higher chlorophyll *a* concentrations than the GFC filters. Phinney and Yentsch (1985) reviewed the degree to which various filter types affected measured chlorophyll *a* concentration and found that GFF and 0.45 micron Millipore filters had similar retention abilities if the chlorophyll *a* concentrations were greater than 1 microgram/liter. Retention efficiencies for GFF and 0.4 micron Nuclepore polycarbonate filters were also compared for samples taken in the NW Atlantic Ocean, and it was found that the Nuclepore filters retained about 12% more chlorophyll *a* than GFF (C. Trees and J. Cullen, unpublished). The selection of filter type obviously affects the precision of pigment measurements and ultimately the accuracy. Although it has been shown, in a few studies, that Nuclepore filters seem to retain more particulates, currently the standard filter recommended under US. JGOFS Protocols is the GFF. This filter was selected to facilitate

comparisons between pigment concentrations and POC, PON, and primary productivity measurements that require the filtration to be on a glass fiber filter. With the development of pigment protocols the precision of the fluorometric method for measuring chlorophyll *a* has improved and is about 5% or better (C. Trees and R. Bidigare, unpublished).

Unfortunately, the accuracy of the fluorometric method has not seen a similar improvement. Phinney and Yentsch (1987) did propose a change in the fluorometric method that would decrease the errors associated with accessory chlorophylls by changing the excitation wavelength. Because this method has only been presented as an abstract and has not been published, it has not accepted even though it greatly improves the method. Using the fluorometric method, errors can be introduced when chlorophylls *b* & *c*, and phaeopigments (chlorophyllide *a* and phaoephorbide *a*) are present (Lorenzen and Jeffrey, 1980). Lorenzen (1981) reported that when there are excessive amounts of chlorophyll *c* relative to chlorophyll *a* , an overestimation of chlorophyll *a* and an underestimation of phaeopigments occurs. The reverse occurs when chlorophyll *b* is present in significant quantities (Loftus and Carpenter, 1971; Gibbs, 1979; Lorenzen and Jeffrey,1980; Vernet and Lorenzen, 1987).

Wide bandpass filters used in the fluorometric method can not differentiate between the various chlorophylls and their associated degradation products. Therefore, the question arises: does the fluorometric method measure only chlorophyll *a* or does it measure some component of the chlorophylls and phaeopigments, since they all contribute to the fluorescence of the sample? Goodwin (1947) and Falk (1964) showed that the fluorescence of a mixture of pigments in dilute solutions (absorbs $\leq 5\%$) is the sum of the fluorescence of the individual components without interaction. Using Lorenzen and Jeffrey's pigment data, Trees *et al.* (1985) showed that the errors associated with the standard fluorometric method are a function of the suite of pigments present in the sample.

Prior to the application of high performance liquid chromatography (HPLC) to phytoplankton pigment analysis, it was difficult to quantitatively measure chlorophylls, carotenoids and chlorophyll degradation products of natural samples. The use of HPLC minimizes the interferences discussed above, since the pigments are physically separated on a column and individually quantified by absorption and fluorescence detectors. HPLC is the method of choice for the quantification of photosynthetic pigments and can be routinely used for phytoplankton pigment analysis (U.S. JGOFS Protocols, 1991).

The variability between the two methods for estimating chlorophyll *a* , for coastal and oceanic samples, was documented by Trees *et al.* (1985) and more recently in data acquired during NASA EOS MODIS experiments and cruises (Clark, 1993). Plots of the fluorometeric vs. HPLC measured chlorophyll *a* data, with their associated least squares regression lines, for eleven cruises are shown in Figure 3 illustrating the geographical variability in this relationship. When the entire data set (2,396 pairs) are combined the linear regression shows almost a 1 to 1 correspondence between two methods (Figure 4) with the fluormetric method under estimating chlorophyll *a* by 7%.

The existing CZCS pigment algorithms (chlorophyll *a* + phaeopigment *a*) were developed using the standard fluorometric method. It is important to continue with these measurements in order to provide a direct link to past CZCS pigment algorithms, as well as assisting in CZCS and MODIS derived products comparison on a global basis.

CZCS Fluorescence.

Fluorescence measurements were made to determine vertical and long-track profiles of chlorophyll *a* pigments. The long-track profiles were made by continuous recording on a strip chart the fluorescence measured by the Turner Model 111 fluorometer fitted with a flow-though cuvette. For station vertical profiles, fluorescence was measured in whole water samples collected using a submersible pump and the same fluorometer. Fluorescence units reported in the report are in arbitrary fluorometer units corrected for the scale expansion (or door factor).

CZCS Phytoplankton Pigments.

About 500 ml of water, depending on phytoplankton standing stock, was filtered through Whatman GFC glass fiber filters to retain chlorophyll *a* containing organisms. The filtered material was extracted using a tissue grinder and 90% acetone-water for determination of the fluorescence before and after the addition of dilute hydrochloric acid (Yentsch and Menzel, 1963; Holm-Hansen *et al.*,1965). chlorophyll *a* and total

pigments were calculated from the fluorescence readings before Rb band after Ra acidification as

$$\text{chlorophyll } a = F_d \frac{\tau}{\tau - 1}(R_b - R_a)\frac{v}{V} \tag{4}$$

$$\text{Phaeopigments } a = F_d \frac{\tau}{\tau - 1}(\tau R_b - R_a) \tag{5}$$

where, $\frac{v}{V}$ is the ratio of volume of the acetone extract to the volume of water filtered. Total pigments are the sum of the chlorophyll *a* and phaeopigment *a* concentration. The acid ratio (τ) is the ratio of fluorescence of pure chlorophyll *a* before and after degradation of the chlorophyll to phaeophytin following acidification, and F_d is the door factor.

The fluorometer was calibrated for τ and F_d before and after each cruise by D.A. Keifer (University of Southern California) using cultured phytoplankton stocks from which chlorophyll *a* was determined by the spectrophotometric tri-chromic method (Richards with Thompson, 1952) as outlined in Strickland and Parsons(1972).

CZCS Total Suspended Matter.

Total suspended particulates were determined by E.T. Baker (NOAA/PMEL) by filtering 1 to 2 liters of water through preweighed 0.45 μm pore size polycarbonate filters. Sea salts were carefully removed from the filters using three 5 ml washes of deionized water, the filters dried in a desiccator, and stored in petri dishes. Their weights were later determined ashore on a 7-digit precision electrobalance. Suspended organic materials were determined from the same filters by oxidizing the organic materials in each sample in 15% hydrogen peroxide solution for 24 hours and reweighing. The weight difference of the oxidized filters and their initial tare is reported as the inorganic suspended materials.

MODIS Pigment Methods.

The procedures described below will be used for all MODIS related pigment measurements. Samples will be filtered through 0.7 micron GFF glass fiber filters and stored in liquid nitrogen. They will then be extracted in 90% acetone and divided for analysis between the HPLC and fluorometric methods. An internal pigment standard (canthaxanthin, which is not normally found in samples) is added to the 90% acetone to correct for volume changes during the extraction process. Since canthaxanthin is a carotenoid and does not fluoresce, it does not affect the fluorometric analysis. The standard fluorometric method of HolmHansen *et al.* (1965) will be used to calculate chlorophyll *a* and phaeopigment concentrations.

The HPLC method used is that proposed by Wright *et al.* (1991). Pigments are separated on the ODS-2 C18 column using a three solvent gradient system at a flow rate of 1 ml per min. The separation of the various pigments requires about 30 minutes with the pigment peaks being detected using two absorption detectors measuring absorption at 404, 436 and 450 nm. In addition, a fluorescence detector (E_x 404, E_m 680) is used to detect and quantify the various chlorophyll degradation products, which usually occur at very low concentrations. The presence of all-vinyl chlorophyll *a* , which co-elutes with chlorophyll *a* , is minimized using the 436 nm absorption data.

Dr. R. Bidigare (University of Hawaii, unpublished) has shown that at naturally occurring concentrations of di-vinyl chlorophyll *a* an error of up to 6-8% in chlorophyll *a* concentration would occur at this wavelength. Since 436 and 450 nm are measured simultaneously for the chlorophyll *a* di-vinyl chlorophyll *a* peak, and each compound absorbs differently at these two wavelengths, it is possible to correct for the di-vinyl chlorophyll *a* contamination by monitoring changes in this ratio as a function as the di-vinyl percentage changes. This approach requires that a di-vinyl chlorophyll *a* standard is available and that a mixture of samples with different relative contributions of di-vinyl chlorophyll *a* to chlorophyll *a* can be run.

Dr. Bidigare provides such a standard to the MODIS experiment team. The precision, measured by the coefficient of variation (Std Dev/Mean$\times$100), at which HPLC can be calibrated for a series of chlorophylls and carotenoids has been found to range from 3-4% (R. Bidigare) to 8% (C. Trees). This precision is a function of the type of detectors and integrators used, as well as the HPLC method. Accuracy for each pigment compound is based on availability of pigment standards and the selection of pigment specific extinction coefficients. Intercalibration exercises between various laboratories has helped to improve this accuracy. Overall, a value of about 5% is probably an appropriate estimate of currently obtainable accuracy, with chlorophyll *a* accuracy being in the 1% level.

MODIS Total Suspended Matter and Organic/Nitrogen.

Water Sampling. Water is collected in the appropriate size bottle to allow sufficient water to filter for both mass determinations and C/N analysis. Geographical location and depth of the euphotic zone will determine the volume needed. Generally, 2-4 liters for oceanic surface waters and 0.5-2 liters for neritic waters. If possible, twice the volume should be used for mass as used for C/N determinations. It is preferable to sample the same depth several times versus using bottle subsamples. Every effort should be made, regardless of bottle size, to have the water well mixed before samples are drawn. The bottle dregs often contain a large portion of the particulate material and care must be taken to include these in the subsamples.

Filtration. Mass Determinations - A 47 mm, 0.45 μm pore size is used. Millipore membrane (MF) or Nuclepore polycarbonate filters are best suited for this analysis. Desiccate and tare filters to a constant weight are measured to tenths of a microgram and placed in individual 47 mm petri dishes. Water can be either pressure or vacuum filtered at 10-7 psi, and the total volume is recorded. We use bottled breathing air. Filters are gently rinsed with a pH adjusted, with respect to sea water, glass distilled water. Two to three quick rinses minimize mass losses due to cell lysis and remove the salts. Filter edges are also rinsed to remove salts. Millipore manufactures a filter (HA EP 047 OW) that has a hydrophobic (non-wetting) edge that eliminates the need for this step and reduces the potential loss of material. After sample collection, filters are folded, gently creased and returned to the petri dish. Filters are dried and not frozen for storage. A dedicated drying oven is used for both mass and carbon/nitrogen filters. Twelve hours are sufficient with the oven at 58-60 C°. A higher temperature will decompose some of the more volatile organic compounds and melt the petri dish.

Carbon/Nitrogen Analysis. Water is filtered through a 25mm Whatman glass fiber GF/F having a nominal pore size of 0.7 μm. The filter is ashed in a muffle furnace at 500-510 C° for at least 2 hours. After the ashing step, each filter is placed in an ashed aluminum lined petri dish. The Control Equipment Elemental Analyzer used requires that the glass fiber filters be encased in protective sleeves. This is accomplished by ashing these and placing them in the petri dish along with the filter. Water is pressure filtered. No rinsing is necessary but the filters are cut in half and placed in the protective nickel sleeves. If a large fraction of the plankton in the collected water are calcarious forming organisms, filters are treated with a dilute hydrochloric acid or sulfuric acid solution to remove inorganic carbon. The filters are then dried in the oven and transported for analysis. The oven used for drying is not used for drying other organic material during this step because of contamination problems. We use a Gelman 25 mm in-line stainless steel filter holder connected to a tubulation bottle that is pressurized with the bottled air. This system can process 6 separate samples at once and can be used for collection for both determinations by changing filter holders.

Bio-Optical Algorithm Formulation

CZCS Bio-Optical Algorithms.

The initial CZCS results reported by Gordon *et al* (1980), demonstrated an excellent potential for achieving the CZCS goal of measuring phytoplankton pigment concentrations to within about a factor of 2. The pigment retrievals, when compared to the shipboard measurements, yielded an agreement to better than 0.5 in $\log_{10}$C, where C is the sum of the chlorophyll *a* and phaeopigment *a* pigments in mg/m^3. In general, within their comparison there appears to be a trend towards under estimating the pigment concentration with the CZCS algorithms. A source for this understanding lies within the preliminary pigment algorithm itself. This bias was corrected by recasting the preliminary pigment algorithms with the addition of data from post-launch validation cruises into forms which are specific to this remote sensing application and the CZCS spectral characteristics. The purpose of implementing these modifications was two-fold: to reduce the sources for systematic bias in estimating the pigment concentrations, and to provide a computation which incorporates the depth dependence of the optical signal and the variations in the vertical distribution of phytoplankton.

Phytoplankton pigment algorithms, for example, require an accurate determination of water leaving spectral radiance. Actually, only the spectral character needs to be retrieved accurately, since within this algorithm scheme only radiance ratios at different wavelengths are used, resulting in some reduction of errors. The radiance ratios are related empirically to the sum of the photosynthetically active phytoplankton

pigment chlorophyll *a* and phaeopigment *a* , its associated degradation product (herein designated by C). The pigment algorithms were developed from measurements whose geographic distributions are depicted in Figure 5. Modifications of the preliminary forms consist of propagating the subsurface radiances to and through the sea surface, weighting the spectral radiance measurements to approximate the CZCS spectral bands, and introducing an optically dependent weighting of the vertical distribution of C. A description of the optical weighting function is discussed in the following section.

Optical Weighting Function For Pigment Stratification.

Distributions of marine phytoplankton within the water column can be highly variable. This variability coupled with the wavelength dependent attenuation character of water, poses a number of serious questions as to the meaningfulness of deriving C from its influence on upwelled spectral radiance. For example, over what depth is the measurement representative of C? A discussion by Gordon and McCluney (1975) demonstrated that for a homogeneous ocean, approximately 90% of the backscattered irradiance available for remote detection emanated from above a depth (z) where the downwelling irradiance falls to about 36% of its value at the surface. This depth is the inverse of the downwelled spectral irradiance attenuation coefficient K_E (m^{-1}) and called the penetration depth. Their work serves as a first approximation in determining the optically significant depth for remote sensing. However, when algorithms involve combinations of radiance at wavelengths, it is unclear which z_{90} should be used. Also, the potential for non-uniqueness in the optical signatures due to stratification of the phytoplankton concentration may limit or render impossible any measurements of C with useful accuracy or precision. Several cases modeled by Duntley *et al* (1974), demonstrated that the subsurface spectral diffuse reflectance was ambiguous as a measure of the total chlorophyll *a* present in the water column. However, the results from various at-sea bio-optical experiments (Kiefer and Austin, 1974; Morel and Prieur, 1977; Smith and Baker, 1977; Morel, 1980; Gordon and Clark, 1980 and Clark *et al*, 1980) implied a high degree of covariation between the inherent and apparent optical properties with the near-surface pigment concentration. Based upon these results, it is obvious that the vertical distributions of C should be weighted by a function which takes into consideration that material near the surface is optically more important than that at greater depths. This function is found by noting the exponential attenuation of irradiance with depth and assuming that the back scattered energy would be approximately attenuated in the same manner on its return to the surface. Thus a layer of material at depth z will have its optical contribution reduced by the factor $e^{2K_E z}$, compared to a similar layer at the surface. Hence, the vertical distribution of C should be weighted spectrally with the function $f(z) = e^{2K_E z}$, where the spectral downwelled irradiance attenuation coefficient is calculated using Equation (1) by substituting the downwelled spectral irradiance $E_d(\lambda, z)$ for $L_u(\lambda, z)$. The optically weighted pigments $C_{f\lambda}(z)$ are then defined by

$$C_{f\lambda} = \frac{\int_0^{z_{90}} C(z) f(\lambda, z) dz}{\int_0^{z_{90}} f(\lambda, z) dz} \tag{6}$$

This procedure has been evaluated theoretically by Gordon and Clark (1980b) and it is shown that $C_{f\lambda}$ should be an accurate representation of the pigment concentration which would be measured by a remote sensor viewing a stratified ocean.

The possibility of the introduction of variance due to including the effects of vertically structured pigments through $C_{f\lambda}$ is particularly interesting. The effect of this was investigated by regressing the surface C versus $C_f(520)$. These data, plotted with their least-squares regression line, are depicted in Figure 6. This regression reveals the rather surprising result that no statistically significant difference exists between the surface and $C_f(520)$ for 55 data pairs. One hypothesis which would explain this result is that the depth $z_{90}(520)$ falls within the mixed surface layer and the variations of C are small. A cursory review of vertical profiles of C, temperature, and computed $K_E(520)$ confirmed this hypothesis and demonstrate that, in this data set, strong variations in C are beginning to occur near $z_{90}(520)$ with $f(z)$ exponentially limiting their contribution on $C_f(520)$.

Initial CZCS Pigment Form.

The at-sea measurements of $L_u(\lambda)$ and C carried out in the manner described above from the pre- and post-launch validation cruises were converted to $L_w(\lambda)$ and $C_f(520)$ as described above. The upwelled radiances at CZCS spectral bands were then formed into the ratios c, $\frac{L_w(443)}{L_w(520)}$, $\frac{L_(520)}{L_w(550)}$, and $\frac{L_w(520)}{Lw(670)}$. The ratio of $\frac{L_w(520)}{Lw(670)}$ was included for use in the high turbidity cases when $t(443)L_w$ approached zero (Gordon

and Clark, 1980a). The ratios and optically weighted (at 520 nm) pigment data were log transformed and subjected to a linear regression analysis. Plots of these data with their associated regression lines are presented in Figure 7. The statistics for these linear regressions are summarized in Table 1. The statistics indicate a good fit to the data with best fits for $\frac{L_w(443)}{L_w(520)}$ and $\frac{L_(520)}{L_w(550)}$, which have standard error of estimates in $\log C_f(520)$, $s_y.x$, of +0.22.

$$\log_{10} C_f(520)(\mathrm{mg/m^3}) = \log_{10} a + b \log_{10} L_w(\lambda_1)/Lw(\lambda_2) \tag{7}$$

TABLE 1.

Summary of Optically Weighted Pigment Concentrations ($\mu g/l$) *vs.* CZCS Water-leaving Radiance Ratios

$\log(C_f^{520})_{mg/m^3} = \log a + b \log(L_w(\lambda_1)/L_w(\lambda_2))$				
statistic	$L_w(443/550)$	$L_w(443/520)$	$L_w(520/550)$	$L_w(520/670)$
a	-0.116	-0.259	0.229	1.642
b	-1.329	-1.806	-4.449	-1.372
s_a	±0.030	±0.036	±0.033	±0.013
s_b	±0.058	±0.094	±0.119	±0.075
$s_{y.x}$	±0.224	±0.262	±0.218	±0.264
r^2	0.908	0.874	0.913	0.876
N	55	55	55	49

MODIS Bio-optical Algorithms.

The initial MODIS bio-optical algorithms will follow the CZCS analog in which the sea surface spectral radiance ratios are related empirically to the parameter of interest, i.e., sum of the photosynthetically active phytoplankton pigment chlorophyll *a* and phaeopigment *a* , chlorophyll *a* , and total suspended matter, at the optimum spectral regions. A preliminary analysis of the in-water optical data has specifically focused on the spectral characteristics of the Sea Star SeaWiFS instrument using a spectral band weighting function from the CZCS instrument and the optically weighted pigments. An additional solar normalization modification has been implemented for this analysis. The normalization removes the solar zenith angle and earth/sun distance dependencies. The relationship between the water-leaving radiances and the normalized radiances is expressed as

$$L_w = L_{wn} \cos\theta_0 e^{-[(0.5\tau_r + \tau_{\mathrm{OZ}})/\cos\theta_0]} \{1 + e\cos[2\pi(D-3)/365]\}^2 \tag{8}$$

where θ_0 is the solar zenith angle, τ_r and τ_{OZ} are, respectively, the Rayleigh and ozone optical thickness. The bracketed term accounts for the variation of distance between the earth and sun, where D is the Julian day and e is the eccentricity of the earth's orbit (0.016).

A test set of pigment algorithms with these modifications were formulated in order to evaluate the modifications and the increase in spectral information. Single and multiple band ratios and optically weighted (at 520 nm) pigment data are being evaluated. A subset of these data plots data with their associated least squares regression lines are presented in Figures 8-12. The statistics for these regressions are summarized in Table 2. The statistics indicate a good fit to the data with best fits for $L_{wn}(490)/L_{wn}(555)$, case I waters and surprisingly, $L_{wn}(445+490+510)/L_{wn}(555)$, case 1 and case 2, which have standard error of estimates in $\log C_f(520)$, $s_y.x$, of +0.185 and +0.221 respectively.

$$\log_{10} C_f(520)(\mathrm{mg/m^3}) = B_0 + B_1 \log_{10} R_{ijk} + B_2 \log_{10} R_{ijk}, \tag{9}$$

where, C is the optically-weighted pigments (520 nm), B_0 the log-log intercept, B_j the log-log regression coefficients and R_{ijk} the ratios of L_{wn} solar normalized radiances (Radiances convolved to the CZCS 520 nm band pass for SeaWiFS simulations).

The approximated CZCS base line algorithm $L_{wn}(445)/L_{wn}(555)$ (Fig. 8) resulted in a small degradation but no statistically significant difference when compared to the CZCS case I form reported by Gordon *et.*

TABLE 2.

Summary of Optically Weighted Pigment Concentrations ($\mu g/l$) *vs.* SeaWiFS Solar Normalized Water-Leaving Radiance Ratios

	R_{ijk}	$S_{y\cdot x}$	r^2	N
case 1	$R(445/555)$	0.203	0.888	35
	$R(510/555)$	0.253	0.826	35
	$R(490/555)$	0.185	0.907	35
case 1 & 2	$R(490/555)$	0.361	0.737	54
	$R(\frac{445+490+510}{555})$	0.221	0.904	53

al. (1983). The recasted pigment algorithm explains from 89% of the variance in $\log_{10}$ pigments over three orders of magnitude in pigment concentration and is accurate to $\pm 1/4$ in log of pigment concentration as compared to 96% in Gordon et. al.(1983).

The basic form which satisfies all of the MODIS bio-optical at-launch products is

$$\log \text{ Product} = A(\log X)^3 + B(\log X)^2 + C(\log X) + D/E, \tag{10}$$

where, A,B,C,D and E are least-squares regression coefficients or constants, and

$$X = \frac{(e)L_{wn}(\text{band 9, 443 nm}) + (f)L_{wn}(\text{band 10, 490 nm}) + (g)L_{wn}(\text{band 11, 530 nm})}{L_{wn}(\text{band 12, 550 nm})}. \tag{11}$$

Here the constants e, f, and g are 0 or 1 and are used to select the spectral bands employed to derive the specific product. The following preliminary coefficient table is based on the original CZCS experimental database adjusted for the SeaWiFS bandwidths. These coefficients will be revised prior to launch for the MODIS spectral band characteristics and the inclusion of new bio-optical database.

TABLE 3.

Preliminary Regression and Band Selection Coefficients.

Product	A	B	C	D	E	e	f	g
log(Pigment) CZCS	0	0	-1.27	0.5	1	1	0	0
log(Pigment) SeaWiFS	-0.63	4.43	-11.2	8.73	1	1	1	1
log(Chl a)	0	0	-1.40	0.07	1	1	0	0
log(Diffuse Attn.)	-0.15	1.44	-4.53	3.56	1	1	1	1

This form accommodates up to four principle wavelength bands which are employed in the empirical derivation of bio-optical products in either single or multiple wavelength ratios. It will be used to generate the following at-launch products for Case 1 waters:

CZCS Pigments (chlorophyll *a* plus phaeopigments)
MODIS Pigments (chlorophyll *a* plus phaeopigments)
chlorophyll *a*
Diffuse Attenuation Coefficient (490nm)

The recasting of the CZCS forms of the phytoplankton pigment algorithms, in terms which are believed to be more representative for SeaWiFS and MODIS applications, has resulted in only minor deviations

from the original analysis. Particularly significant is that the multiple band ratios will provide a robustness not possible with the CZCS's limited spectral information. The future inclusion of the Marine Optical Characterization Experimental data which will considerably expand the diversity of pigments and water masses sampled and should provide the data required to assess whether an overall improvement in accuracy results from the modified algorithm form. This is the subject of the present SeaWiFS calibration/validation effort.

References

Austin, R.W., *The Remote Sensing of Spectral Radiance from below the Ocean Surface*, Optical Aspects of Oceanography (N.G. Jerlov and E. Steeman Nielsen, eds.), Academic Press, London, 1974, pp. 317–344.

———, *Gulf of Mexico, Ocean Color Surface-Truth Measurements*, Boundary-Layer Meteor. **18** (1980), 269–285.

———, *Coastal Zone Color Scanner Radiometry*, Ocean Optics 6 (Seibert Q. Duntley, ed.), SPIE, vol. 208, 1980, pp. 170–177.

Ball Brothers Research Corporation, *Development of the Coastal Zone Color Scanner for Nimbus-7, Vol. 2: Test and Performance Data, Final Report F78-11*, Ball Brothers Research Corporation, 1979, p. 93.

Clark, D.K., Baker, E.T., and Strong, A.E., *Upwelled Spectral Radiance Distribution in Relation to Particulate Matter in Sea Water*, Boundary-Layer Meteor. **18** (1980), 287–298.

Duntley, S.Q., Austin, R.W., Wilson, W.H., Edgerton, C.F. and Moran, S.E., *Ocean Color Analysis*, Scripps Institution of Oceanography Ref. 74-10, p. 70 yr 1974.

Falk, J.E., *Spectra.*, Porphyrins and Metalloporphyrins (J.E. Falk, ed.), Elsevier, New York, 1964, pp. 85–88.

Gibbs, C.F., *Chlorophyll b interference in the fluorometric determination of chlorophyll a and "phaeopigments*, Aust. J. Mar. Freshwater Res. **30** (1979), 597–606.

Goodwin, R.H., *Fluorometric method for estimating small amounts of chlorophyll a*, Anal Chem. **19** (1947), 789–794.

Gordon, H.R. and Clark, D.K., *Atmospheric Effects in the Remote Sensing of Phytoplankton Pigments*, Boundary-Layer Meteor **8** (1980a), 300–313.

———, *Remote Sensing Optical Properties of a Stratified Ocean: An Improved Interpretation*, Applied Optics **8** (1980b), 3428–3430.

Gordon, H.R., Clark, D.K., Mueller, J.L. and Hovis, W.A., *Phytoplankton Pigments Derived from the Nimbus-7 CZCS: Initial Comparisons with Surface Measurements*, Science **210** (1980), 63–66.

Gordon, H.R. and McCluney, W.R., *Estimation of the Depth of Sunglint Penetration in the Sea for Remote Sensing*, Applied Optics **14** (1975), 413–416.

Hovis, W.A., Clark, D.K., Anderson, F., Austin, R.W., Wilson, W.H., Baker, E.T., Ball, D., Gordon, H.R., Mueller, J.L., El-Sayed, S.Z., Strum, B., Wrigley, R.C., and Yentsch, C.S., *Nimbus-7 Coastal Zone Color Scanner: System Description and Initial Imagery*, Science **210** (1980), 60–63.

Holm-Hansen, O., C.J. Lorenzen, R.W. Holmes and J.D.H. Strickland., *Fluorometric determination of chlorophyll*, J. Cons. Cons. Int. Explor. Mer. **30** (1965), 3–15.

Kiefer, D.A. and Austin, R.W., *The Effect of Varying Phytoplankton Concentration on Submarine Light Transmission in the Gulf of California*, Limnol. Oceanogr **19** (1974), 55–64.

JGOFS Core Measurement Protocols, Rpt. of the Core Measurement Working Groups, SCOR, ICSC, 1991.

Loftus, M.E. and J.H. Carpenter, *A fluorometric method for determining chlorophylls a, b, and c*, J. mar. Res. **29** (1971), 319–338.

Lorenzen, C.J., *Chlorophyll b in the eastern North Pacific Ocean*, Deep Sea Res. **28A** (1918), 1049–1056.

Lorenzen, C.J. and S.W. Jeffrey, *Determination of chlorophyll in seawater*, Unesco Tech. Pap. in Mar. Sci. **35** (1980), 20.

Morel, A., *In-Water and Remote Measurements of Ocean Color*, Boundary-Layer Meteor **18** (1980), 177–201.

Morel, A. and Prieur, L., *Analysis of Variations in Ocean Color*, Limnol. Oceanogr **22** (1977), 709–722.

Phinney, D.A. and C.S. Yentsch, *A novel phytoplankton chlorophyll technique: toward automated analysis*, J. Plk. Res **7(5)** (1985), 633–642.

———, *Fluorometric techique for the determination of phytoplankton chlorophyll a and phaeopigments in the presence of accessory chlorophylls*, Trans. Am. Geophys. Union **EOS 68(50)** (1987), 1706.

Smith, R.C. and Baker, K.S., *The Bio-Optical State of Ocean Waters and Remote Sensing*, Scripps Institution of Oceanography Ref. 77-2, 1977, p. 36.

Strickland, J.D.H. and T.R. Parsons, *A Practical Handbook of Seawater Analysis*, Fisheries Res, vol. Bulletin 167, Board of Canada, Ottawa, 1972, p. 311.

Trees, C.C., M.C. Kennicutt and J.M. Brooks, *Errors associated with the fluorometric determination of chlorophylls and phaeopigments*, Marine Chemistry **16** (1985), 1–12.

Vernet, M. and C.J. Lorenzen., *The presence of chlorophyll b and the estimation of phaeopigments in marine phytoplankton*, J. of Plank. Res. **9(2)** (1987), 255–265.

Wright, S.W., S.W. Jeffrey, R.F.C. Mantoura, C.A. Llewellyn, T. Bjornlan D.Repeta and N. Welschmeyer, *Improved HPLC method for the analysis of chlorophylls and carotenoids from marine phytoplankton*, Mar. Ecol. Prog **Ser. 77** (1991), 83.

Yentsch, C.S. and D.W. Menzel, *A method for the determination of phytoplankton, chlorophyll, and phaeophytin by fluorescence*, Deep-Sea Res. **10** (1963), 221–231.

Figure Captions

Figure 1. Schematic for the typical spectral radiometric observations.

Figure 2. Comparison between two different chlorophyll *a* measurement protocols: GF/C filters vs. GF/F filters.

Figure 3. A series of geographically variable data illustrating the covariation between fluorometric vs. HPLC methods of measuring chlorophyll *a* concentrations.

Figure 4. HPLC determined chlorophyll *a* vs. fluorometrically determined chlorophyll *a* with the combined data set (2396 stations). The least-square fit for the data set is also shown.

Figure 5. Ship station locations at which data were acquired for the bio-optical algorithms. Circled stations had chlorophyll concentrations less than 0.3 mg/m^3.

Figure 6. $\log_{10}$ of the concentration of optically weighted pigments, $\bar{C}_f^{520}$ (mg/m^3), within the first penetration depth ($Z^\lambda \approx 90\%$, where $\lambda = 520$ nm) versus $\log_{10}$ of surface pigments, C (mg/m^3). The equation for the least-square regression line shown with these data is $\log_{10} C = -0.034 + 1.012 \log_{10} \bar{C}_f^{520}$.

Figure 7. $\log_{10}$ of the concentration of optically weighted pigments, $\bar{C}_f^{520}$ (mg/m^3), within the first penetration depth ($Z^\lambda \approx 90\%$, where $\lambda = 520$ nm) versus $\log_{10}$ of surface upwelled radiance ratios (L_w^{443}/L_w^{550}, L_w^{443}/L_w^{520}, L_w^{520}/L_w^{550}, L_w^{520}/L_w^{670} and the least-square regression lines.

Figure 8. $\log_{10}$ of the concentration of optically weighted pigments, $\bar{C}_f^{520}$ (mg/m^3), versus $\log_{10}$ of solar normalized water leaving radiance ratio for case 1 waters, L_w^{445}/L_w^{555} and the least-square regression line.

Figure 9. $\log_{10}$ of the concentration of optically weighted pigments, $\bar{C}_f^{520}$ (mg/m^3), versus $\log_{10}$ of solar normalized water leaving radiance ratio for case 1 waters, L_w^{510}/L_w^{555} and the least-square regression line.

Figure 10. $\log_{10}$ of the concentration of optically weighted pigments, $\bar{C}_f^{520}$ (mg/m^3), versus $\log_{10}$ of solar normalized water leaving radiance ratio for case 1 waters, L_w^{490}/L_w^{555} and the least-square regression line.

Figure 11. $\log_{10}$ of the concentration of optically weighted pigments, $\bar{C}_f^{520}$ (mg/m^3), versus $\log_{10}$ of solar normalized water leaving radiance ratio for case 1 and case 2 waters, L_w^{490}/L_w^{555} and the least-square regression line.

Figure 12. $\log_{10}$ of the concentration of optically weighted pigments, $\bar{C}_f^{520}$ (mg/m^3), versus $\log_{10}$ of solar normalized water leaving radiance ratio for case 1 and case 2 waters, $L_w^{445+490+510}/L_w^{555}$ and the least-square regression line.

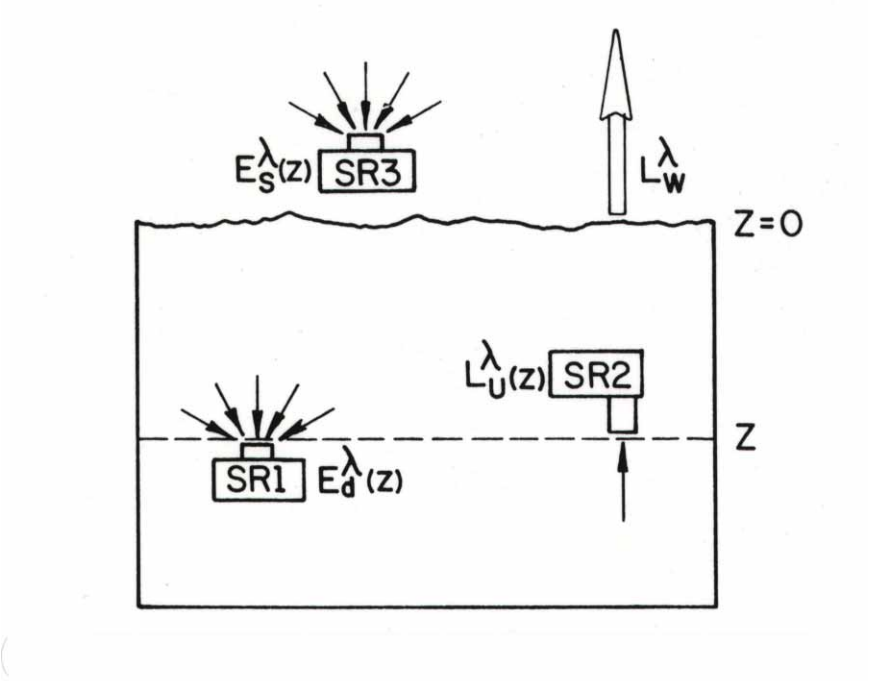

FIGURE 1.

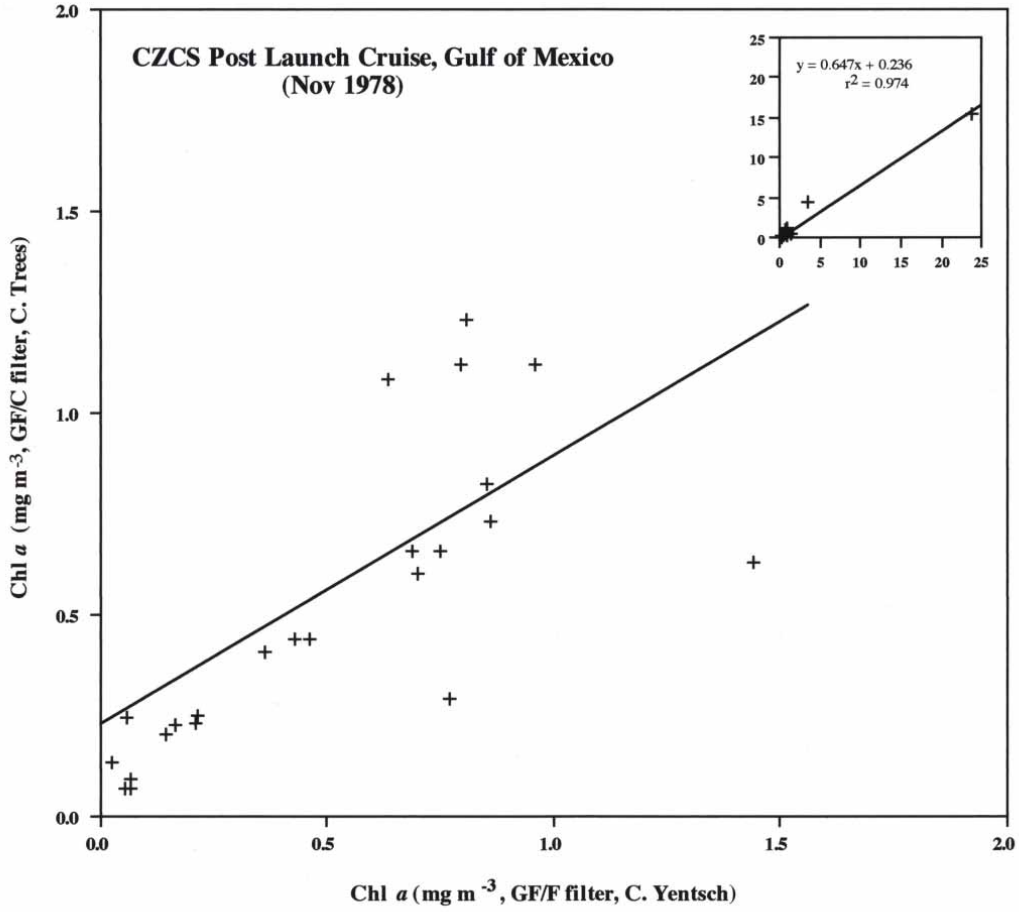
CZCS Post Launch Cruise, Gulf of Mexico
(Nov 1978)
y = 0.647x + 0.236
r2 = 0.974
Chl a (mg m-3, GF/C filter, C. Trees)
Chl a (mg m-3, GF/F filter, C. Yentsch)
0.0
0.5
1.0
1.5
2.0
0
5
10
15
20
25

FIGURE 2.

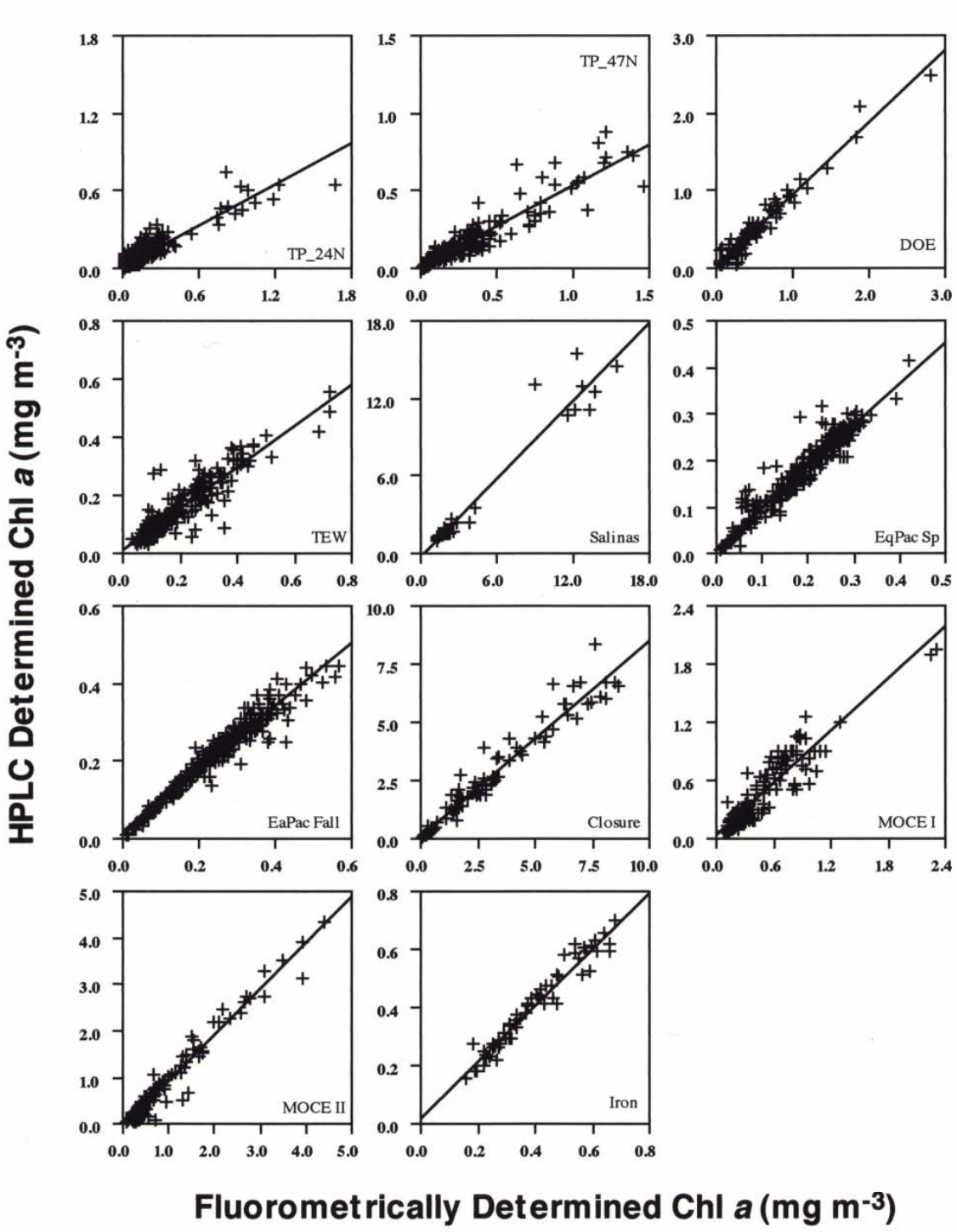
HPLC Determined Chl a (mg m-3)
Fluorometrically Determined Chl a (mg m-3)
TP_24N
TP_47N
DOE
TEW
Salinas
EqPac Sp
EaPac Fall
Closure
MOCE I
MOCE II
Iron

FIGURE 3.

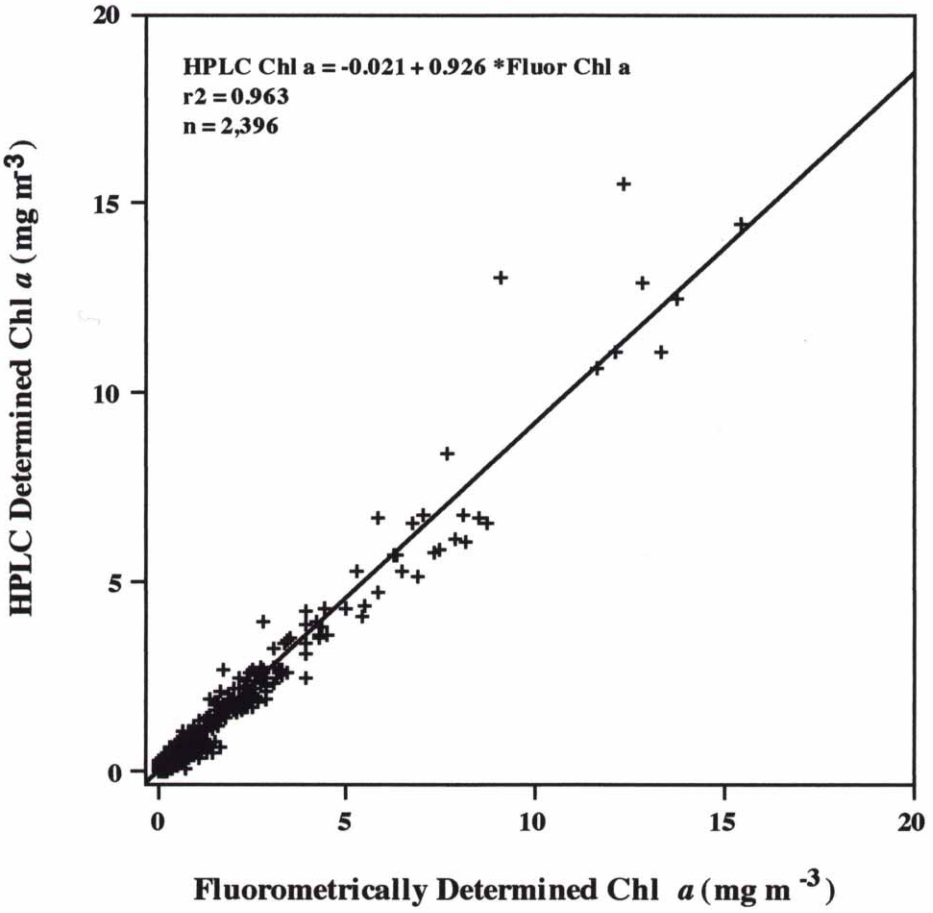
HPLC Chl a = -0.021 + 0.926 *Fluor Chl a
r2 = 0.963
n = 2,396
HPLC Determined Chl a (mg mr3)
Fluorometrically Determined Chl a (mg m -3)
0
5
10
15
20

FIGURE 4.

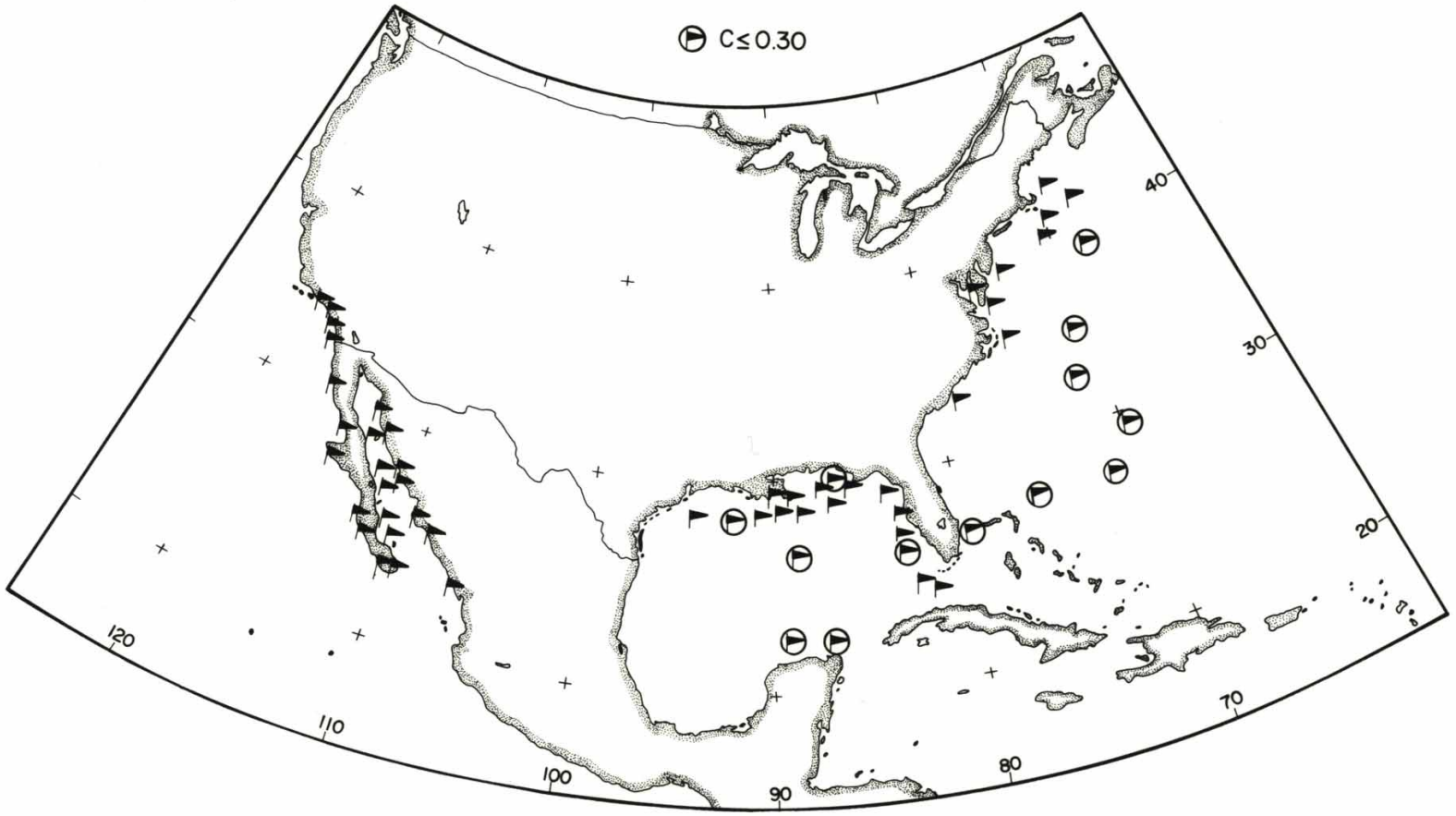

FIGURE 5.

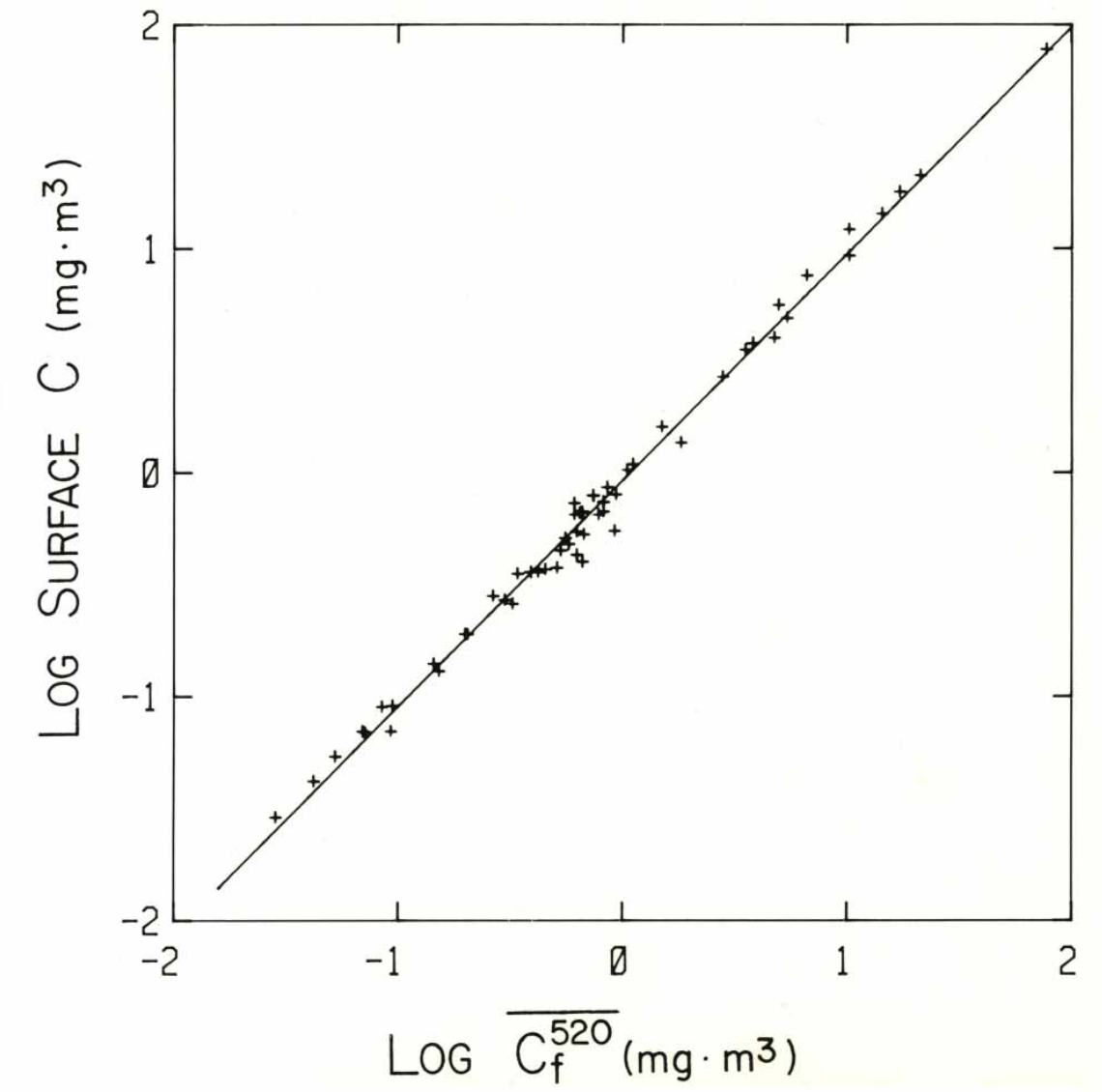

FIGURE 6.

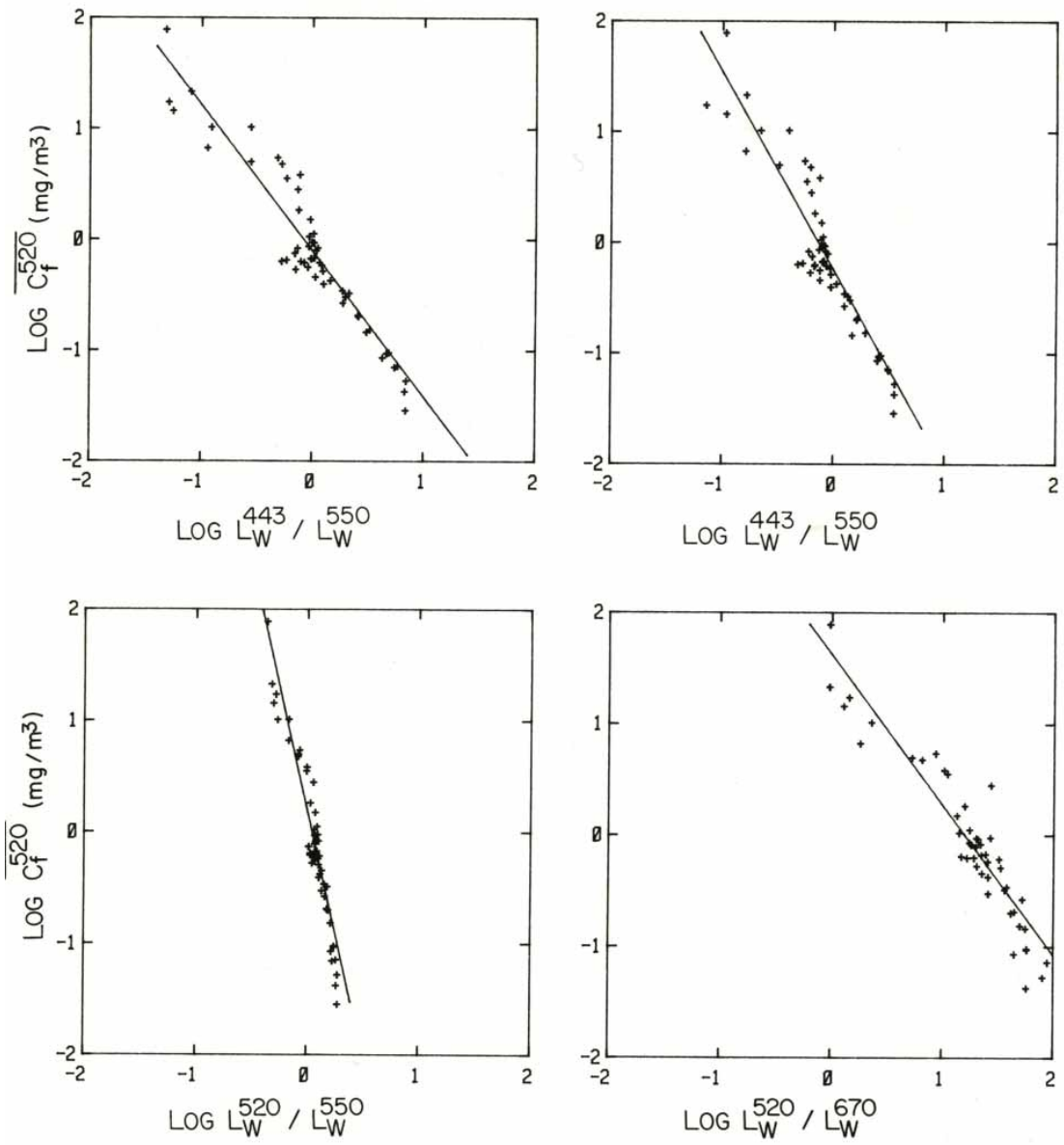
LOG $\overline{C_f^{520}}$ (mg/m³)
LOG L_W^{443} / L_W^{550}
LOG L_W^{443} / L_W^{550}
LOG $\overline{C_f^{520}}$ (mg/m³)
LOG L_W^{520} / L_W^{550}
LOG L_W^{520} / L_W^{670}

FIGURE 7.

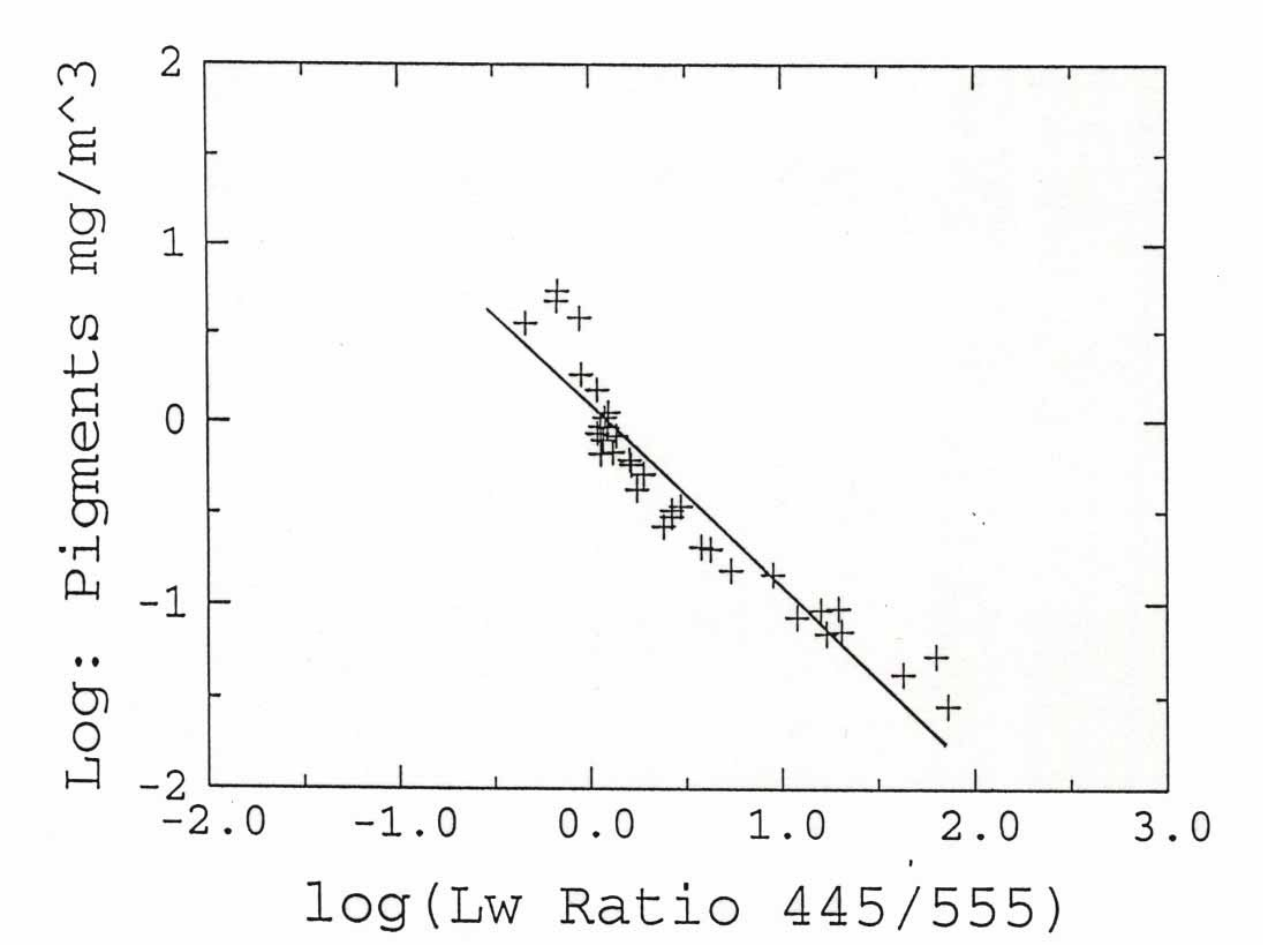

FIGURE 8.

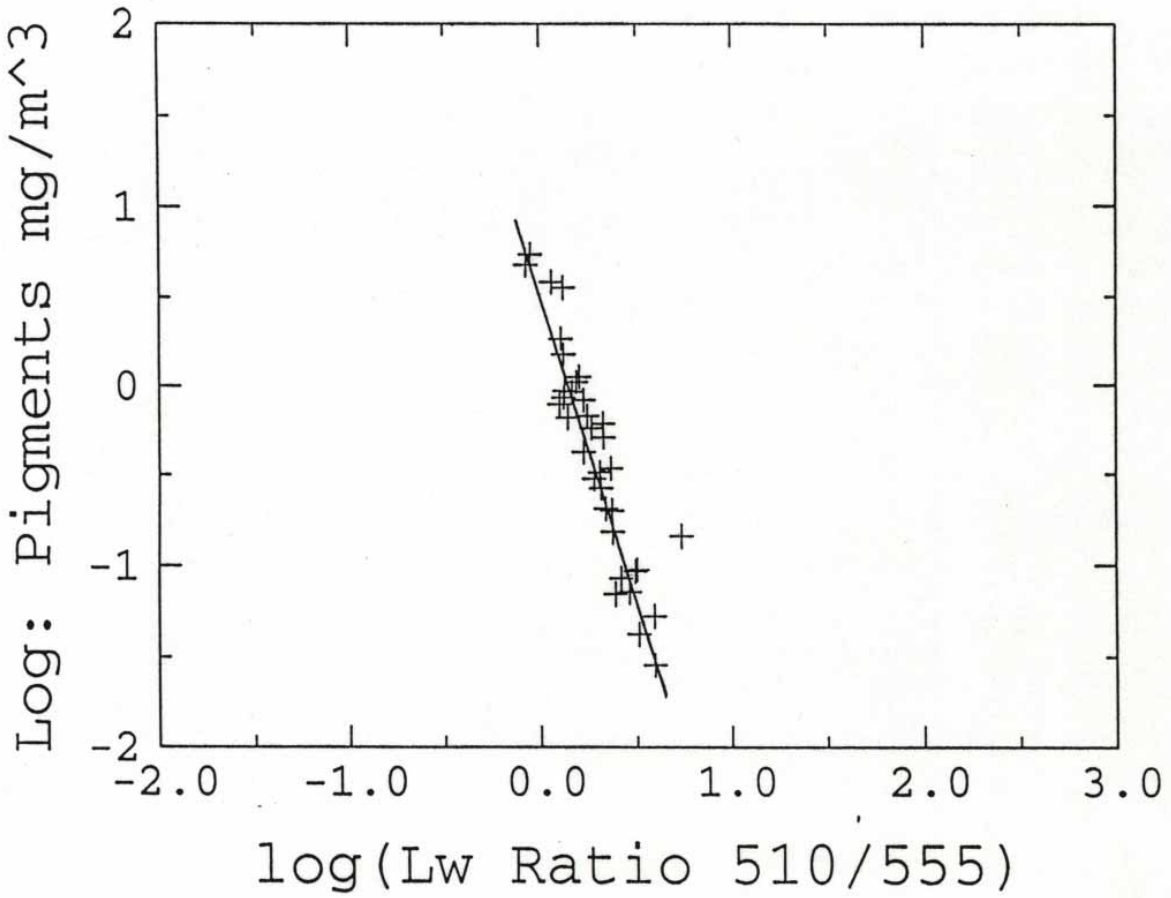

FIGURE 9.

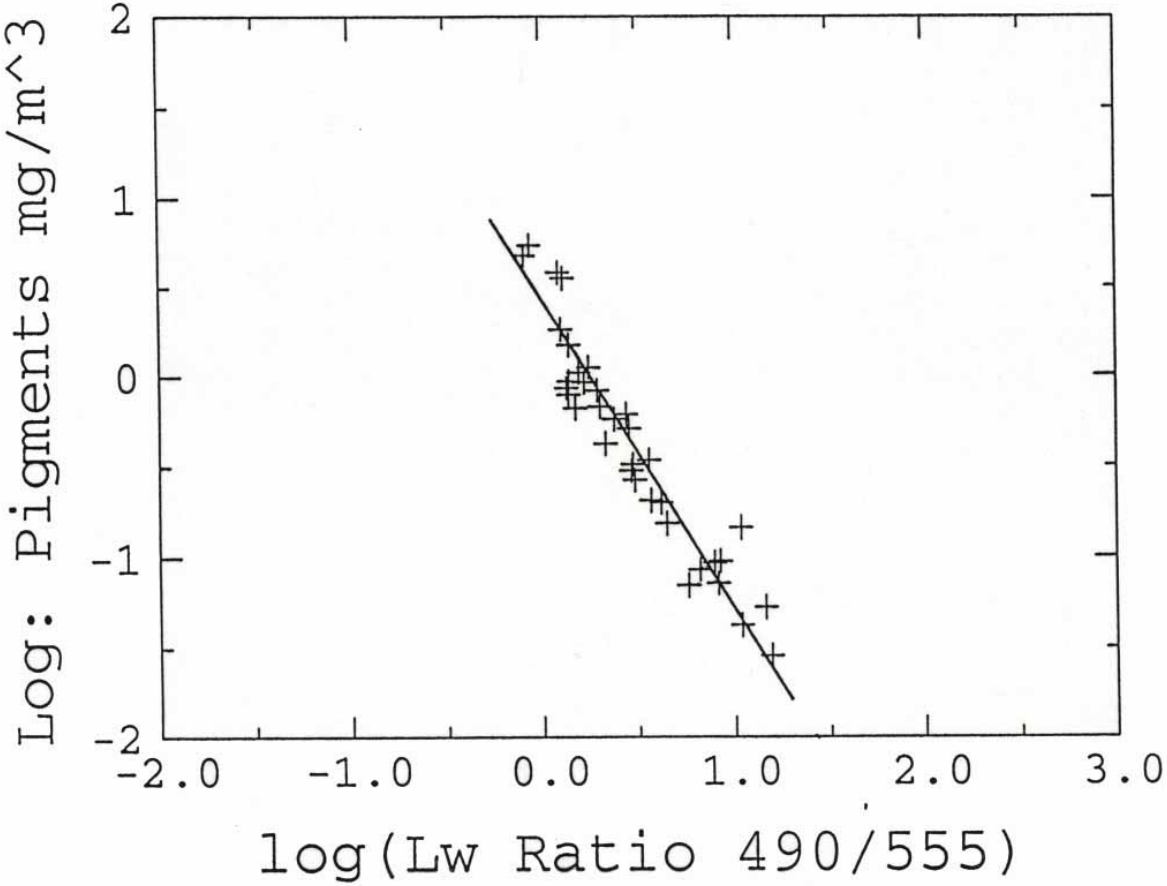

FIGURE 10.

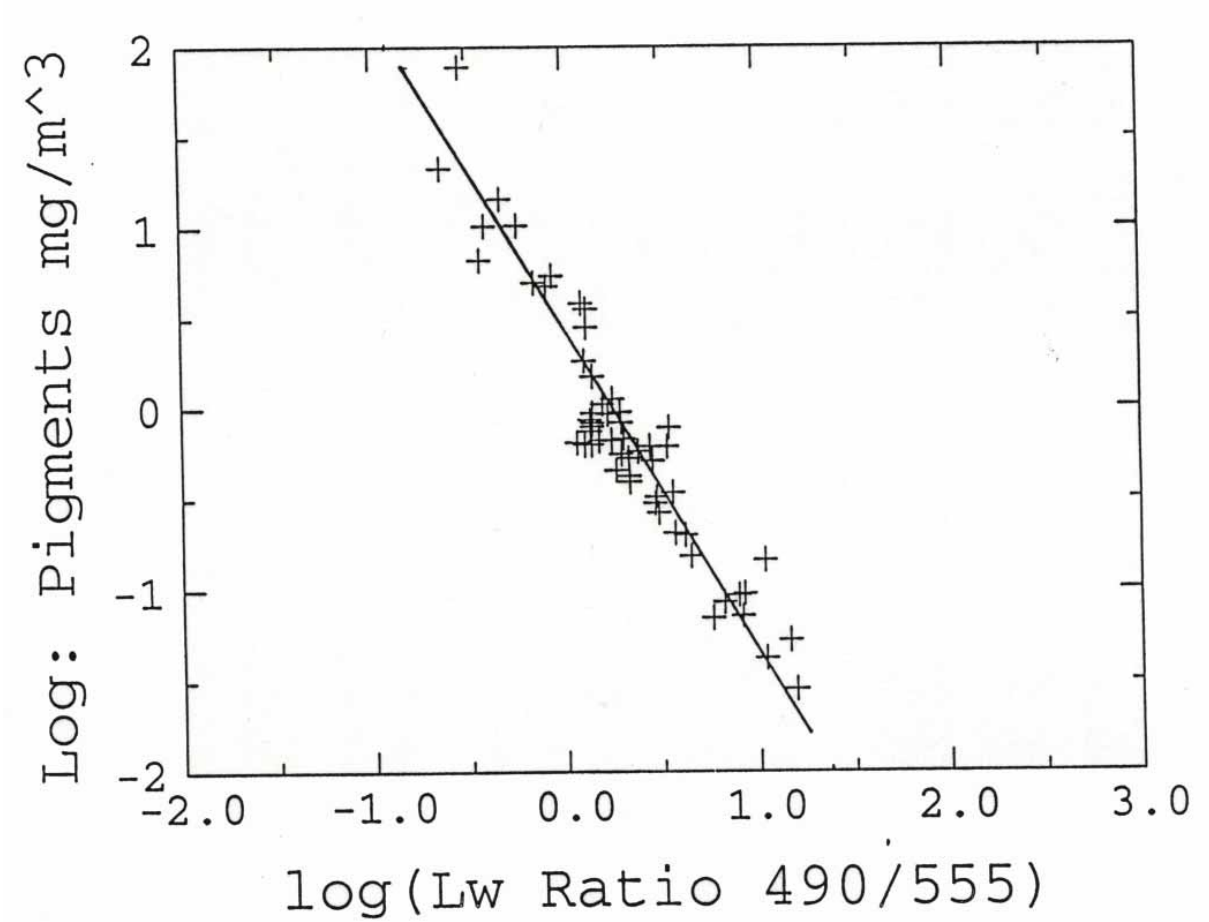

FIGURE 11.

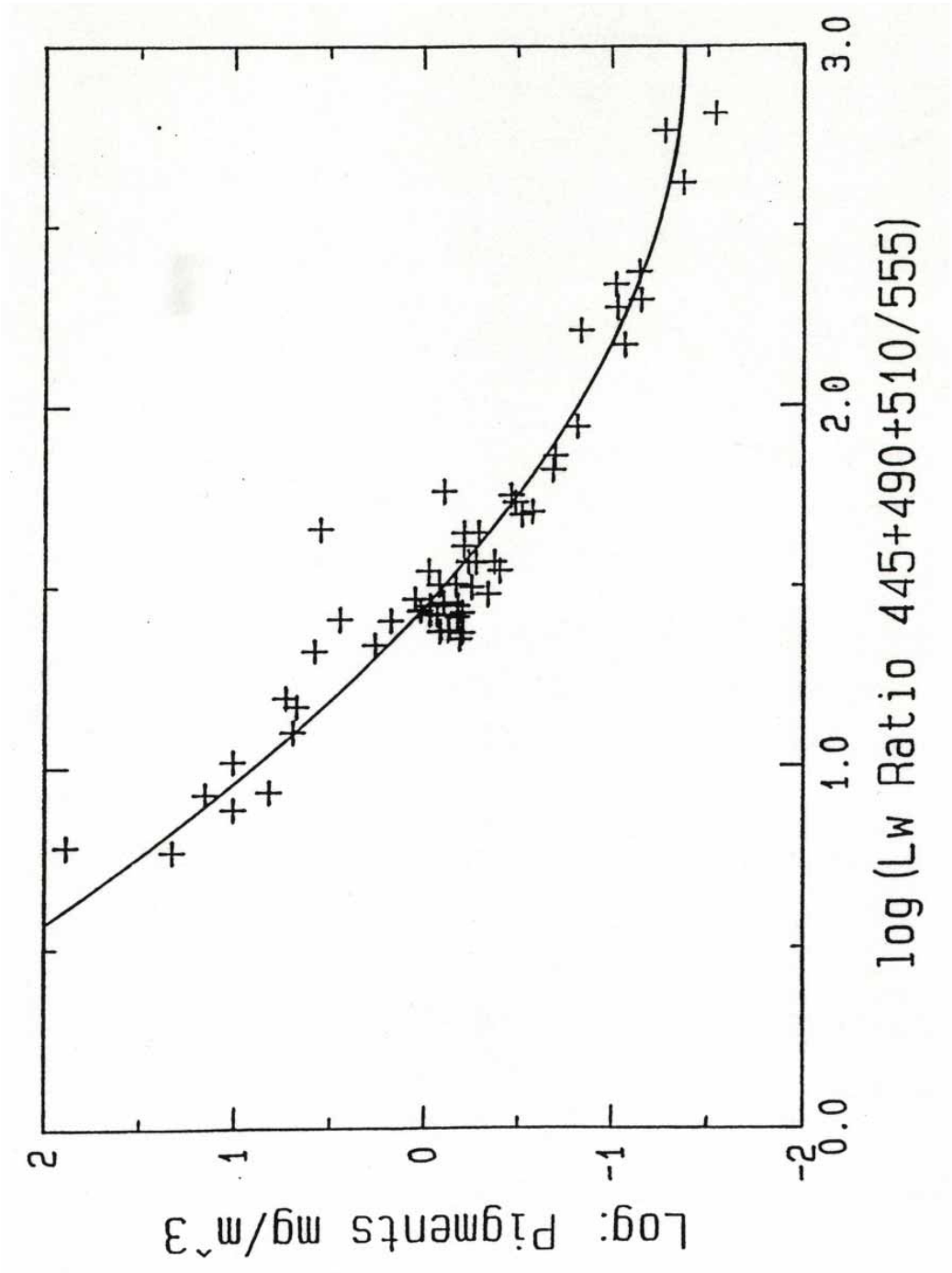
Log: Pigments mg/m^3
2
1
0
-1
-2
0.0
1.0
2.0
3.0
log (Lw Ratio 445+490+510/555)

FIGURE 12.

Presented at the
Aerosol Remote Sensing Workshop
Sponsored by NASA/EOS
April 15–19, 1996
Washington, D.C.

Validation of Atmospheric Correction over the Oceans

by

D. K. Clark[1], H.R. Gordon[2], K.J. Voss[2],
Y. Ge[3], W. Broenkow[4], and C. Trees[5]

[1] NOAA/NESDIS, Camp Springs, MD 20746

[2] Department of Physics, University of Miami, Coral Gables, FL 33124

[3] Research and Data Corporation, Greenbelt MD, 20770

[4] Moss Landing Marine Laboratories, San Jose State University, Moss Landing, CA 95039

[5] CHORS, San Diego State University, San Diego, CA 92120

Acknowledgment

This work received support from the National Aeronautics and Space Administration under Contracts NAS5-31363 and S-19864-E.

Abstract

By validation of atmospheric correction, we mean quantification of the uncertainty expected to be associated with the retrieval of the water-leaving radiance from the measurement of the total radiance exiting the ocean-atmosphere system. This uncertainty includes that associated with the measurement or estimation of auxiliary data required for the retrieval process, e.g., surface wind speed, surface atmospheric pressure, and total Ozone concentration. For a definitive validation, this quantification should be carried out over the full range of atmospheric types expected to be encountered. However, funding constraints require that the individual validation campaigns must be planned to address the individual components of the atmospheric correction algorithm believed to represent the greatest potential sources of error. In this paper we develop a strategy for validation of atmospheric correction over the oceans. We also provide a detailed description of the instrumentation and methods that have been developed for implementation of the plan.

1. Introduction

Atmospheric correction of ocean color imagery is discussed in detail by *Gordon* [1996] (this meeting). Briefly, in atmospheric correction one attempts to remove the contribution to the radiance L_t measured by the sensor that results from scattering in the atmosphere and reflection from the sea surface. If carried out correctly, the result is the water-leaving spectral radiance, $L_w(\theta_v, \phi_v, \lambda)$, where θ_v and ϕ_v are, respectively, the polar and azimuth angles of a vector from the point on the ocean being examined (pixel) to the sensor, and λ is the wavelength. This is related to the upward radiance just beneath the sea surface $L_u(\theta'_v, \phi'_v, \lambda)$, where θ'_v and θ_v are related by Snell's law, and $\phi'_v = \phi_v$, i.e.,

$$L_w(\theta_v, \phi_v, \lambda) = \frac{T_F(\theta'_v, \theta_v)}{m^2} L_u(\theta'_v, \phi'_v, \lambda), \tag{1}$$

where m is the index of refraction of water, and T_F is the Fresnel transmittance of the air-sea interface. In an attempt to remove the effects of atmospheric transmission and the solar zenith angle, [Gordon *and* Clark 1981] defined the normalized water-leaving radiance, $[L_w(\theta_v, \phi_v, \lambda)]_N$:

$$L_w(\theta_v, \phi_v, \lambda) = [L_w(\theta_v, \phi_v, \lambda)]_N \cos\theta_0 \exp\left[-\left(\frac{\tau_r(\lambda)}{2} + \tau_{OZ}(\lambda)\right)\left(\frac{1}{\cos\theta_0}\right)\right], \tag{2}$$

where $\tau_r(\lambda)$ and $\tau_{Oz}(\lambda)$ are the optical thickness of the atmosphere associated with molecular (Rayleigh) scattering and Ozone absorption, respectively, and θ_0 is the solar zenith angle at the specific pixel. The exponential factor partially accounts for the attenuation of solar irradiance by the atmosphere. Ignoring bidirectional effects [Morel *and* Gentili 1991] , the normalized water-leaving radiance is approximately the radiance that would exit the ocean in the absence of the atmosphere with the sun at the zenith. This quantity is used in other algorithms to derive ocean-related properties, e.g, the chlorophyll concentration. Often it is useful to replace radiance by reflectance. The reflectance ρ associated with a radiance L is defined to be $\pi L/F_0 \cos\theta_0$, where F_0 is the extraterrestrial solar irradiance. The normalized water-leaving radiance is converted to normalized water-leaving reflectance $[\rho_w]_N$ through

$$[\rho_w]_N = \frac{\pi}{F_0}[L_w]_N. \tag{3}$$

The goal of atmospheric correction of the Moderate Resolution Imaging Spectroradiometer (MODIS) [Salomonson et al. 1989] is to retrieve $[\rho_w(\theta_v, \phi_v, \lambda)]_N$ at 443 nm with an uncertainty less than ± 0.002. This corresponds to an uncertainty of $\sim \pm 5\%$ at 443 nm in $[\rho_w(\theta_v, \phi_v, \lambda)]_N$ for very clear waters, e.g., the Sargasso Sea in summer [Gordon *and* Clark 1981] . In this paper we discuss the validation of the atmospheric correction procedure.

By the term validation of atmospheric correction, we mean quantification of the uncertainty expected to be associated with the retrieval of $[\rho_w(\theta_v, \phi_v, \lambda)]_N$ from the measurement of the total radiance (reflectance) exiting the ocean-atmosphere system. This uncertainty includes that associated with the measurement or estimation of auxiliary data required to operate the correction algorithm, e.g., surface wind speed, surface atmospheric pressure, total column Ozone concentration. For a proper validation, this quantification should be carried out over the full range of atmospheric and water types expected to be encountered in the retrievals.

2. Our approach to validation

Gordon [1996] (this meeting) shows that in the open ocean far from the influence of land (and in the absence of the long-range transport of dust) and/or anthropogenic aerosol sources, where the atmosphere is very clear and the aerosol is located in the marine boundary layer, a simple single-scattering correction algorithm should be sufficient to provide $[\rho_w(\theta_v, \phi_v, \lambda)]_N$ with the desired accuracy at 443 nm. For more turbid atmospheres, in which multiple scattering is important, [Gordon *and* Wang 1994a] developed an algorithm that uses a set of candidate aerosol models developed by [Shettle *and* Fenn 1979] to assess the effects of multiple scattering. This algorithm performs well as long as the absorption properties of the candidate aerosol models are similar to the actual aerosol present in the atmosphere. Furthermore, if the aerosol is non-absorbing or weakly absorbing, the algorithm is insensitive to the vertical distribution of the aerosol. However, difficulties with this algorithm can occur under certain conditions, one of which is when the aerosol is strongly absorbing. In this case, the successful operation of the algorithm still requires that the candidate aerosol models be representative of the actual aerosol present, and in addition, that the thickness of the layer in which the dominant aerosol resides must be known or estimated with an accuracy of $\sim \pm 1$ km.

Based on these observations, it is reasonable to focus the atmospheric correction validation on regions dominated by (1) a locally generated maritime aerosol, and (2) strongly absorbing aerosols. In this manner it is possible to establish an uncertainty estimate characteristic of regions for which the atmospheric correction should be excellent, and to estimate how the uncertainty increases in regions with aerosols that present correction problems.

The open ocean, free of land and anthropogenic sources, represents the most favorable of conditions for atmospheric correction. In such a region, the aerosol is locally generated and resides in the marine boundary layer. In the absence of intense stratospheric aerosol, as might be present following a volcanic eruption, and in the absence of thin cirrus clouds, only whitecaps and residual sun glitter need to be removed in order that conditions satisfy those assumed in the development of the correction algorithm, i.e., a relatively clear two-layer atmosphere with aerosols in the lower layer. Under such conditions, the error in the water-leaving radiance due to the aerosol removal should be small, and specifying this component of the error field under these conditions relatively simple. When the error due to the aerosol is small, errors due to whitecaps and sun glitter may make a significant contribution to the overall error, therefore, a location with the conditions described above would be ideal for specifying the error fields due to these processes. The site chosen for such validation is in the waters off Hawaii.

There are two common situations with strongly absorbing aerosols in which the atmospheric correction algorithm may not retrieve the water-leaving radiances within acceptable error limits: situations in which the aerosol absorption is relatively independent of wavelength (urban aerosols transported over the oceans); and situations in which the aerosol absorption has significant dependence (desert dust transported over the oceans). Clearly, it is important to perform validation in regions and times where significant amounts of both types of absorbing aerosol are expected to be present over the water. In the case of urban pollution an ideal location is the Middle Atlantic Bight during summer (excellent logistics as well). For desert dust there are two important regions: the North Pacific (Gobi desert influence) and the Tropical North Atlantic (Saharan desert influence). We plan a validation cruise in the Tropical North Atlantic.

In order to utilize imagery in the more turbid Case 2 waters near coasts, it is critical to understand the limitations that significantly higher (than typical oceanic) concentrations of suspended particulate matter in the water place on atmospheric correction. Thus, validation of atmospheric correction should also be carried out in a coastal region of spatially varying turbidity. Such a validation can be effected in the Middle Atlantic Bight by making measurements at a set of stations successively closer to the coast. In this manner, it will be possible to combine the validation cruises for studying the limitations imposed by urban aerosols and by waters of moderate turbidity.

It is important to examine in detail the influence of stray light from bright targets (ghosting, internally reflected and scattered light, etc.) in the MODIS focal plane fields-of-view, on atmospheric correction. For example, how close can one perform adequate atmospheric correction to a cloud bank or coastline? This can be effected by examining the atmospheric correction in broken cloud fields and near islands in clear

water. The Hawaii optical mooring site (Subsection 4.2) appears to be ideal for such studies. These would provide error bounds on normalized water-leaving radiances under such conditions. This single site should be adequate for assessing this component of the error field.

Validation of any algorithm developed for removal of stratospheric aerosols and/or thin cirrus clouds is also required; however, it will not be necessary to conduct a focussed validation experiment for this purpose. One need only track the quality of the atmospheric correction in the experiments recommended above with regard to the scene reflectance at 1380 nm (used to indicate the presence and amount of stratospheric aerosol and/or thin cirrus) to assess the efficacy of this component of the algorithm.

Finally, an important component of validation is an estimate of the day-to-day consistency and the long-term stability of the retrieved radiances. The Hawaii optical mooring site (Subsection 4.2) will provide the water-leaving radiances required to monitor the quality of the retrievals on a continual basis.

3. Required measurements

Obviously to validate the atmospheric correction it is necessary to compare near-simultaneous satellite-derived and surface-measured values of the retrieved quantity: $[L_w]_N$ or $[\rho_w]_N$. Typically, *in situ* measurements of $L_u(\theta'_v, \phi'_v, \lambda)$ are obtained only for $\theta'_v = 0$, and $[L_w]_N$ is derived for this direction, and used to develop algorithms for relating water-leaving radiance to ocean properties. It has usually been assumed that $L_u(\theta'_v, \phi'_v, \lambda)$ is nearly independent of θ'_v and ϕ'_v. However, recently Morel and coworkers [Morel *and* Gentili 1991; Morel *and* Gentili 1993; Morel, Voss *and* Gentili 1995] have shown that L_u varies considerably, depending on θ'_v, ϕ'_v, θ_0, and ϕ_0, where ϕ_0 is the solar azimuth. Thus, for purposes of validation, one must measure $L_u(\theta'_v, \phi'_v, \lambda)$, i.e., the upwelling spectral radiance just beneath the sea surface in the direction the sensor is viewing. L_w is then determined with Eq. (1). As MODIS views the ocean with a spatial resolution of ~ 1 km at nadir, an assessment of the variability of $L_u(\theta'_v, \phi'_v, \lambda)$ within the pixel under examination must be carried out to obtain a pixel-averaged $L_u(\theta'_v, \phi'_v, \lambda)$.

It is to be expected that in some cases the satellite-derived normalized water-leaving radiances will not agree with the surface measurements within the required error limits. In such cases it will be important to understand what part of the atmospheric correction algorithm is at fault in order to facilitate algorithm "fine tuning." This requires what we term "auxiliary" measurements, i.e., measurements of quantities other than that which is being validated. Several such measurements are discussed next.

Since the major (highly variable) component to be removed during atmospheric correction is the aerosol, it is important to make detailed measurements of the columnar aerosol optical properties as part of the validation effort. Quantities to be measured include the spectral aerosol optical thickness and the spectral sky radiance, both close to (the aureole) and far from the sun. From such measurements, it is possible to obtain the columnar aerosol size distribution, aerosol phase function and aerosol single scattering albedo, an index of the aerosol absorption [Kaufman et al. 1994; King et al. 1978; King *and* Herman 1979; Nakajima, Tanaka *and* Yamauchi 1983; Wang *and* Gordon 1993] . This data will be used to determine the applicability of the aerosol model selected by the algorithm for use in the atmospheric correction, and to provide a determination of the presence or absence of strongly absorbing aerosols.

As mentioned in Section 2, the correction algorithm is insensitive to the vertical distribution of the aerosol only if it is weakly absorbing or non-absorbing. Thus, an additional possibility for a degradation in the accuracy of the retrieved water-leaving radiances is the presence of significant quantities of absorbing aerosol in the free troposphere. Because of this it is important to be able to assess the vertical structure of the aerosol. The most direct technique of effecting this is LIDAR [Sasano *and* Browell 1989] and such measurements, either ship-borne or air-borne, should be included in validation exercises.

Whitecaps on the sea surface can also result in larger-than-required uncertainty in $[\rho_w(\theta_v, \phi_v, \lambda)]_N$ [Gordon *and* Wang 1994b; Koepke 1984] , unless the increase in the spectral reflectance of the ocean-atmosphere system can be estimated within about ± 0.002. The severity of the whitecap perturbation depends on the spectral form of the reflectance [Frouin, Schwindling *and* Deschamps 1995; Gordon 1996; Schwindling 1995] . Thus, an estimate of the whitecap contribution to the perturbation of the $[\rho_w(\theta_v, \phi_v, \lambda)]_N$ is required.

Finally, the ancillary data required to operate the atmospheric correction algorithm, and, in the processing of MODIS data estimated from numerical weather models, must also be measured. These include surface

atmospheric pressure, wind speed, and wind direction.

4. Instrumentation and measurements

The validation as envisaged will be carried out via ship-based and buoy-based measurements. The ship-based validation will involve the more complete set of measurements, as much of the instrumentation cannot be operated from buoys. We shall discuss each in detail.

4.1 Ship-based instrumentation.

A complete set of measurements for validation of atmospheric correction must be ship-based, as the most fundamental measurement, $L_u(\theta'_v, \phi'_v, \lambda)$, can only be made from such platforms. The basic measurements to be carried out at sea are high spectral resolution ($\sim$ 3–4 nm) measurements of L_u at nadir ($\theta'_v = 0$, actually $\theta'_v < 5°$), measurement of $L_u(\theta'_v, \phi'_v, \lambda)$ in a few spectral bands (full width at half maximum (FWHM) $\sim$ 10 nm), measurement of the augmentation of the water-leaving reflectance by whitecaps, measurement of the aerosol optical thickness (FWHM $\sim$ 4 nm) and sky radiance (FWHM $\sim$ 10 nm) in a few spectral bands, and measurement of ancillary parameters such as surface wind speed and direction and atmospheric pressure at the surface. Instrumentation developed to meet these measurement requirements is described next. Protocols for most of the measurements are provided in [Mueller *and* Austin 1992].

4.1.1 Upwelling spectral radiance at nadir.

Typically, for remote sensing applications, the optical measurements are performed in the near surface waters at three or four depths, z. The selection of these depths depends on the clarity of the water. The optical instrument which measures upwelled spectral radiances $L_u(z, \lambda)$ and downwelled spectral irradiance $E_d(z, \lambda)$ is suspended from a buoy and drifted away from the ship in order to avoid shadowing by the ship. On board the ship, a second spectrometer measures the downwelling sky and sun spectral irradiance just above the sea surface, $E_s(z, \lambda)$, when the submerged spectrometer is at depth z in order to normalize for the variations in the incident irradiance. The shallowest observations of upwelled spectral radiances (nominally one meter) are then propagated upward to just beneath the sea surface by first calculating the upwelled spectral radiance attenuation coefficient $K_L(\lambda)$ using

$$K_L(\lambda) = \frac{1}{z_2 - z_1} \ell n \left[\frac{L_u(z_1, \lambda)}{E_s(z_1, \lambda)} \frac{E_s(z_2, \lambda)}{L_u(z_2, \lambda)} \right], \tag{4}$$

where z_1 and z_2 are the two shallowest depths at which measurements are carried out ($z_1 < z_2$). Then the radiance loss between the surface and z is accounted for through

$$L_u(0, \lambda) = L_u(z_1, \lambda) \exp[K_L(\lambda) z_1]. \tag{5}$$

The subsurface upwelled radiances are then transmitted through the sea surface using Eq. (1) and normalized with Eq. (2). These high resolution spectra may then be convolved with the satellite sensor's spectral response, $S_i(\lambda)$ for band i, to form the band-averaged water-leaving radiance:

$$\langle [L_w(\lambda)]_N \rangle_i = \int S_i(\lambda) [L_w(\lambda)]_N \, d\lambda \tag{6}$$

Examples of spectra of $L_u(z, \lambda)$, acquired during the Marine Optical Characterization Experiment (MOCE-3) conducted during the Fall of 1994 in Hawaiian waters, are presented in Figure 1a along with derived attenuation coefficients and water-leaving radiances in Figure 1b.

Since effective application of ocean color satellite observations, to derive bio-optical products, rely totally on retrieving accurate and precise water-leaving radiances, a new marine optical instrumentation and a buoy system to enhance its in-situ measurement capability has been developed. A prototype Marine Optical System (MOS) has been constructed and tested. The operational version of this system is now in its final construction phase and is scheduled for at-sea test and evaluation during the summer of 1996. The system uses a modular design concept which has provided a high degree of flexibility and has facilitated the ease

in which instrument upgrades can be implemented. The concept was constrained by the buoy requirement that necessitated the instrument be capable of maintaining measurement integrity while being unattended for long periods of time. This constraint has led to a design which minimizes the number of moving parts (one) and has resulted in the spectrographic application of concave holographic diffraction gratings. These spectrograph gratings approximate a flat focal field to the degree that planar silicone photodiode arrays may be used as detectors. Inherent within this technology are the features of simplicity, compactness, durability, and stable high performance system characteristics. The new operational version uses a convex holographic grating spectrograph with a cooled CCD detector system. These modifications are being implemented in order to improve image quality, dynamic range, and signal to noise ratios. Additionally, the shipboard system is being modified to utilize fiber-optics to avoid the instrument self shadowing errors as described by [Gordon *and* Ding 1992]. An overview of the salient features of this system is provided in Table 1.

Laboratory radiometric calibrations are performed prior to and after each deployment. Spectral standards for irradiance are either NIST traceable or NIST standard lamps (1000 W FEL'S). NIST protocols for irradiance calibrations are used in conjunction with commercial systems (EG&G GAMMA Scientific (Model 5000) and Optronics Model 420) which have integrating spheres for radiance calibrations. During the laboratory calibrations, portable reference lamps are measured and then utilized during the at-sea deployments to provide a time history of the system response stability. For the buoy system a submersible reference lamp has been developed for divers to perform monthly checks of the system's stability. Wavelength calibrations are performed with five low pressure lamps, which provide numerous emission lines over the instruments spectral range.

4.1.2 Upwelling spectral radiance distribution.

The spectral upwelling radiance distribution $L_u(z, \theta'_v, \phi'_v, \lambda)$ will be measured using a radiance distribution camera system (RADS) [Voss 1989; Voss *and* Chapin 1992] . This system employs a fisheye camera lens to image the upwelling radiance distribution onto a thermoelectrically cooled CCD camera (First Magnitude, Starscape IIb). Included in the optical path are interference filters which are used to select the spectral region of interest. There are four possible filter positions on each of two filter wheels which can be used to obtain the upwelling radiance distribution in 6 different spectral bands. Since only the near surface radiance distribution is needed in this application, the instrument will be deployed by suspending it beneath a float at the depth z_L of 1.5 to 2 meters. This will allow the instrument to drift away from the ship and avoid ship shadow contamination of the data [Gordon 1985] . Data reduction and instrument calibration are performed using standard procedures which have been described elsewhere [Voss *and* Zibordi 1989] . $L_u(z_L, \theta'_v, \phi'_v, \lambda)$ will be propagated to the surface using K_L derived from the nadir-viewing MOS (Subsection 4.1.1). This is acceptable as $L_u(z, \theta'_v, \phi'_v, \lambda)$ decays with depth in a manner that is a weak function of θ'_v and ϕ'_v. If necessary, the radiance distribution will be interpolated between spectral bands using the L_u at nadir spectrum discussed in the last paragraph.

4.1.3 Whitecap reflectance contribution.

To determine the whitecap contribution to the top-of-the-atmosphere reflectance, a new radiometer system has been constructed [Moore, Voss *and* Gordon 1996] . This instrument system consists of a narrow field-of-view radiometer, video camera system, downwelling irradiance sensor, wind speed and direction instruments, and a GPS receiver. The radiometer and irradiance sensor have 6 spectral bands each, with matching filters to enable the upwelling reflectance of the sea surface to be calculated. The radiometer and video camera system are aligned to view the same scene and deployed 5–10 m in front of the bow of the ship to obtain a downward view of the surface uncontaminated by ship wake effects even while the ship is underway. The full angle field-of-view of the radiometer is approximately 1°, so the diameter of the surface sampling area is typically 20 cm (depending on the height of the bow above the sea surface). The video camera signal is recorded and the images are time stamped to allow synchronization of the video images and radiometer data. The video images are useful for identifying whitecaps and other surface features in the data stream, e.g., sun glitter. The data from the radiometer, irradiance sensor, and wind speed and direction instrument are digitized at 1000 Hz, and the average of 100 samples are recorded at 0.5 Hz along with the GPS position. By continuously measuring the total reflectance of the ocean surface, the whitecap contribution to the signal may be determined. Samples in the data stream, with and without whitecaps, can be found, and therefore

the overall reflectance with, and without, whitecaps can be determined. Since the relative wind speed, direction, and ship heading and speed are also recorded, a relationship between the true wind speed and whitecap augmentation of the reflectance can be found.

4.1.4 Aerosol optical thickness.

The aerosol optical thickness is measured using a standard sun photometer [d'Almeida et al. 1983] . The total optical thickness, τ, is given by the relationship,

$$\tau = -\frac{1}{m}\ell n\left(\frac{E_m}{E_0}\right), \tag{7}$$

where E_m is the direct solar irradiance measured in instrument units (such as counts) with the sun photometer, E_0 is the calibrated extraterrestrial solar irradiance in instrument units, and m is the air mass. For solar zenith angles, θ_0, less than 60°, m is very close to $1/\cos\theta_0$ [Kasten *and* Young 1989]), it can be determined precisely from the solar ephemeris with the measurement of time and position. The E_0 is determined for the sun photometer through a Langley calibration [Shaw 1983] . The total optical depth is determined in spectral bands which do not have sharp molecular absorption bands. In this manner the only other components, besides aerosols, which have significant contributions are the molecular (Rayleigh) scattering and the broad Chappiux absorption band of Ozone. Thus once the total optical thickness is determined, the aerosol optical thickness can be found by subtraction of the Rayleigh optical thickness, determined by calculation [Young 1980] , and the ozone optical thickness, determined by ozone climatologies [Klenk et al. 1983] , or by direct measurement, and knowledge of the wavelength dependence of ozone absorption [Nicolet 1981; Vigroux 1953] . A sample data set, including both a Langley regression and the reduced optical depths are shown in Figure 2. This data set was collected at sea during the MOCE-3 cruise during the Fall of 1994 near the Island of Hawaii.

4.1.5 Sky radiance.

On land, an automatic pointing instrument, e.g., the Automatic Sun and Sky Radiometer (ASSR) [Holben et al. 1996] may be used to make sky radiance distribution measurements, but on a ship obtaining a stable reference is difficult and expensive. Thus, for our ship-borne program, we will use a camera system similar to the RADS system described above. This fisheye camera system is mounted in a "stable table" which is an active servo-controlled table to maintain its vertical reference. Otherwise the overall system is very similar to the in-water system. Sample data are shown in Figure 3. This data set was collected from the Mauna Wave, off of the MOBY site during October 1995. These contour plots show the radiance distribution for four wavelengths: 440, 560, 670, and 860 nm. The units of the contours are 10^{-2} μW/cm^2/nm/sr. The sky camera can also be equipped with polarizers to enable measurement of the first three elements of the Stokes vector in the sky radiance distribution (the linear polarization components).

Because of the rapid change in sky radiance near the sun, the RADS system requires that a 10° portion of the sky around the sun be blocked to prevent flare in the camera lens system. To acquire the sky radiance near the sun, an important component when the atmospheric single scattering albedo is needed to assess the aerosol absorption, another instrument has been constructed. This instrument, a solar aureole camera system, is designed to measure the sky radiance for the region from 2° to 10° from the solar disk. This instrument is based on a cooled CCD camera system (Spectra source, MCD1000). In this system a 35 mm camera lens (50 mm focal length) is used to image the sky around the sun. An interference filter is attached to the front of the lens to select the spectral region of interest, and a small aperture (1 cm) is placed in front of the interference filter. A small occulting disk is placed approximately a meter in front of the camera and is oriented such that the shadow of this disk falls over the aperture on the interference filter. Thus the direct solar image is blocked from the camera system, yet the area around the sun can be imaged. The system is controlled, via software, to be operated with a push-button on the camera itself. When the shadow of the occulter is in the correct position, the operator triggers the push-button which tells the camera system to operate the shutter then to download the image. Immediately afterward, a dark image is obtained to be used in the data reduction process. Calibration of this system is similar to the RADS system. The calibration procedures required include, camera system roll off and flat fielding, system linearity, absolute

radiance calibration, and spectral calibration. These procedures have been performed as described in [Voss *and* Zibordi 1989].

4.1.6 Phytoplankton pigments.

Normally the measurement of the phytoplankton pigment concentration, C, (defined to be the sum of the concentrations of chlorophyll a and phaeophytin a in the water) is not used in this type of validation process. However, for the very clear water cases (C . 0.25 mg/m^3), the water-leaving radiance spectral variance can be estimated as a function of pigment concentration for λ & 520 nm [Gordon *and* Clark 1981] . In-order to estimate the spatial variability of the surface waters around the primary bio-optical station, a grid of ship tracks is traversed while continuously measuring chlorophyll a fluorescence. A fluorometer, depth sensor, and water pumping system are towed while the ship is underway at near-surface depth (five meters typically). Calibration of the fluorometric signal is conducted from high frequency sampling (every 15 minutes) of the water pumped from the towed depth for laboratory extraction of pigments. Contour maps of the pigment distribution and the estimated normalized water-leaving radiances are then generated for satellite inter-pixel variability analyses. An example of such a pigment map (7.3 × 7.3 km) generated around a station in Hawaiian waters is illustrated in Figure 4. A total of ten transit legs with 19 discrete samples along the legs was acquired to generate this product.

4.1.7 Ancillary measurements.

Apparent wind speed and direction are determined using a standard instrument manufactured by Young Co. (Model 05103). The apparent wind observations are corrected for the ship's heading and speed from the ship's navigation instrumentation (gyro and speed log). Relative humidity and air temperature are measured with Vaisalla sensor systems (Models HMD 30/UB/YB and HMD/W 30YB respectively). Atmospheric pressure is obtained from a digital pressure transducer manufactured by Setra (Model 470). These measurements are all continuously logged at 1hz along with GPS time and position. The data are then processed into mean values at specified time intervals, i.e. mean atmospheric pressure every four hours. Ozone concentrations may be obtained from various sources. For the MOBY site, column ozone can be obtained from the NOAA/CMDL site at Mauna Loa (personal communication, Gloria Koenig, NOAA/CMDL). For other sites in the northern hemisphere data can be obtained from the WMO Ozone Mapping Center. (http://www.athena.auth.gr:80/ozonemaps/) which derives the data from SBUV-2 satellite data and ozone zones around the world.

4.2 Buoy-based instrumentation.

The Marine Optical Buoy System (MOBY), illustrated in Figure 5, is tethered to a slack-line moored main buoy. MOBY is a 15 meter, 2500 lb, wave-rider buoy which emulates an "optical bench" with a 12 meter column extending into the sea. The surface buoy floatation (manufactured by Moorings System Inc.) is 1.7 meters in diameter, with four 40-watt solar panels mounted to the antenna support column. The surface buoy houses the controlling computers, mass storage, electronics, cellular modem, and computer battery. The Marine Optical System discussed in Subsection 4.1.1, has been reconfigured for the buoy application. The instrument along with four 200 amp/hr gelcell marine batteries is located in the subsurface housing at the bottom of the buoy. The apparent optical properties (upwelled radiances and downwelled irradiances) are measured by a series of remote collectors positioned on arms extending away from the central column. The arms may be positioned at varying depths, typically 1.5, 6, and 10 meters, along the column. The E_s sensor is located at the top of the surface buoy. The remote collectors are coupled to 1 mm, multimode fiberoptic cables which are terminated at a fiberoptic rotary selector (multiplexer). This optical multiplexer is mounted to one of the MOS entrance windows. Multiplexer ports are selected and the energy incident on the remote collector relays the light into the MOS optical train and detectors. The optical and ancillary data are relayed to the surface computer and stored on disk for future access via a cellular telephone link. The transmitted data will be converted into calibrated radiances and a water-leaving radiance data base for sensor quality control monitoring and algorithm development.

The selection of the calibration/validation site for MOBY was primarily based upon the clear-water water-leaving radiance criterion [Gordon *and* Clark 1981] , logistics, and survivability. The site selected is located at 20°49.0′N and 157°11.5′ W in 1200 m of water, and is approximately 10 nautical miles from the west

coast of the Hawaiian Island of Lanai (Figure 6). The mountains on the Islands of Molokai, Lanai, and Maui provide a lee from the dominant trade winds (note mean wind speed isopleths in Figure 6). This lee reduces the amount of sea, swell, and cloud cover at the mooring site which increases the probability of mooring survivability and cloud free satellite coverage. Logistics are conducted from a dockside operational support facility which has been constructed at the University of Hawaii's Marine Operations Facility in Honolulu. GTE-MobleNet has excellent cellular coverage in the region, facilitating the transfer of relatively large MOBY observational data sets back to the MOBY support facility computer or to the mainland. University of Hawaii ships are utilized for MOBY deployments and maintenance. The transit time to the MOBY site from Honolulu is approximately six hours, allowing for a relatively quick response time in case emergency service is required.

In support of the MOBY calibration/validation effort, a land-based automatic sun and sky radiometer [Holben et al. 1996] (ASSR, CIMEL Electronique) has been installed at a remote site on the west coast of Lanai at 20°49.57′ N,156°59.1′ W (Figures 6 and 7). The ASSR measures the direct solar irradiance in several wavelength bands (440, 670, 870, 937, 940, and 1020 nm) in the visible every 15 minutes during the morning and afternoon. In addition the instrument measures the sky radiance in the principal plane (the sun-zenith plane) and along the almucantar (the collection of azimuthal angles with the same zenith angle as the sun) in several wavebands (440, 670, 860, and 1020 nm) three times each morning and afternoon. This data is collected automatically, and is sent via the GOES satellite to NASA/Goddard where it can be accessed over the Internet. In its location on Lanai it has an unobstructed view to the south and west for measurement of the sky radiance and the aerosol optical thickness. Volicanic activity on the Island of Hawaii, which lies approximately 165 miles to the southeast of the site, will produce unique aerosol occurrences when the surface winds are from the southeast. The frequency of these wind conditions is approximately ten days per year (J. Porter, University of Hawaii, personal communication). The observations are acquired approximately 11.3 nautical miles from the MOBY site and should be representative of the atmospheric conditions in that region. Shipboard atmospheric measurements will be made for comparison purposes on the MOBY quarterly maintenance cycles.

5. Concluding remarks

We have described the requirements for validating the MODIS atmospheric correction algorithm over the oceans, and presented a plan for effecting the validation. To implement the validation plan, new instrumentation and techniques have been developed, and were briefly described in the text. With few exceptions, the instrumentation required to carry out the plan exists or is in the final phase of testing. We believe that the plan as described will provide a measure of the uncertainty expected to be associated with the atmospheric correction of MODIS. It will also provide data to allow "fine tuning" of the correction algorithm using MODIS data. If carried out, it should allow establishment of the correction uncertainty characteristic of oceanic regions for which atmospheric correction is normally expected to be excellent, and provide an estimate of the increase in uncertainty in settings in which the correction is expected to be degraded. The quality of the validation will be dependent on the extent to which the plan can be carried out.

References

d'Almeida, G.A., R. Roggendorf and D. Richter, *New sunphotometer for network operation*, Applied Optics **22** (1983), 3796–3801.

Frouin R., M. Schwindling and P. Y. Deschamps, *Spectral reflectance of sea foam in the visible and near-infrared: In-situ measurements and implications for remote sensing of ocean color and aerosols, Spectral reflectance of sea foam in the visible and near-infrared: In-situ measurements and implications for remote sensing of ocean color and aerosols*, submitted to Jour. Geophys. Res. (1995).

Gordon, H. R., *Ship Perturbation of Irradiance Measurements at Sea 1: Monte Carlo Simulations*, Applied Optics **23** (1985), 4172–4182.

———, *Atmospheric Correction of Ocean Color Imagery in the Earth Observing System Era*, submitted to Jour. Geophys. Res. (1996).

——— and D. K. Clark, *Clear water radiances for atmospheric correction of coastal zone color scanner imagery*, Applied Optics **20** (1981), 4175–4180.

——— and K. Ding, *Self-Shading of In-Water Optical Instruments*, Limnology and Oceanography **37** (1992), 491–500.

——— and M. Wang, *Retrieval of water-leaving radiance and aerosol optical thickness over the oceans with SeaWiFS: A preliminary algorithm*, Applied Optics **33** (1994a), 443–452.

———, *Influence of Oceanic Whitecaps on Atmospheric Correction of SeaWiFS*, Applied Optics **33** (1994b), 7754–7763.

Holben, B. N., T. F. Eck, I. Slutsker, D. Tanre, J. P. Buis, A. Setzer, E. Vermote, J. Reagan, Y. Kaufman, T. Nakajima, F. Lavenu and I. Jankowiak, *Automatic Sun and Sky Scanning Raiometer System for Network Aerosol Monitoring*, Remote Sensing of Environment (Accepted) (1996).

Kasten, F. and A. T. Young, *Revised optical air mass tables and approximation formula*, Applied Optics **28** (1989), 4735–4738.

Kaufman, Y. J., A. Gitelson, A. Karnieli, E. Ganor, R. S. Fraser, T. NakaJima, S. Mattoo and B. N. Holben, *Size distribution and scattering phase functions of aerosol particles retrieved from sky brightness measurements*, Jour. Geophys. Res. **99D**, 10341–10356.

King, M. D., D. M. Byrne, B. M. Herman and J. A. Reagan, *Aerosol size distributions obtained by inversion of optical depth measurements*, Jour. Atmos. Sci. **35** (1978), 2153–2167.

——— and B. M. Herman, *Determination of the Ground Albedo and the lndex of Absorption of Atmospheric Particulates by Remote Sensing. Part I: Theory*, Jour. Atmos. Sci. **36** (1979), 163–173.

Klenk, K. F., P. K. Bhartia, E. Hilsenrath and A. J. Fleig,, *Standard ozone profiles from balloon and satellite data sets*, J. Climate and Appl. Meteorology **22** (1983), 2012–2022.

Koepke, P., *Effective Reflectance of Oceanic Whitecaps*, Applied Optics **23** (1984), 1816–1824.

Moore, K. D., K. J. Voss and H. R. Gordon, *Measurements of the Spectral Refiectance of Whitecaps in the Open Ocean*, EOS, Transactions, American Geophysical Union, vol. 76, OS105, 1996.

Morel, A. and B. Gentili, *Diffuse reflectance of oceanic waters: its dependence on Sun angle as influenced by the molecular scattering contribution*, Applied Optics **30** (1991), 4427–4438.

———, *Diffuse reflectance of oceanic waters. II. Bidirectional aspects*, Applied Optics **32** (1993), 6864–6879.

———, K. J. Voss and B. Gentili, *Bidirectional reflectance of oceanic waters: A comparison of modeled and measured upward radiance fields*, Jour. Geophys. Res. **100C, 13** (1995), 143-13,150.

Mueller, J. L. and R. W. Austin, *Sea WiFS Technical Report Series: Volume 5, Ocean Optics Protocols for SeaWiFS Validation*, vol. Technical Memorandum 104566, NASA, Greenbelt, MD, July 1992..

Nakajima, T., M. Tanaka and T. Yamauchi, *Retrieval of the Optical Properties of Aerosols from Aureole and Extinction Data*, Applied Optics **22** (1983), 2951–2959.

Nicolet, M., *The solar spectral irradiance and its action in the atmospheric photodissociation processes*, Planet. Space Sci. **29** (1981), 951–974.

Salomonson, V. V., W. L. Barnes, P. W. Maymon, H. E. Montgomery and H. Ostrow, *MODIS: Advanced Facility Instrument for Studies of the Earth as a Syste*, IEEE Geosci. Rem. Sens. **27** (1989), 145–152.

Sasano, Y. and E. V. Browell, *Light scattering characteristics of various aerosol types derived from multiple wavelength lidar observations*, Applied Optics **28** (1989), 1670–1679.

Schwindling, M., Modeles, *et measures pour l'observation spatiale de la couleur de l'ocean: Diffusion atmospherique par les aerosols et reflesion de surface par l'ecume*, Docteur de L'Universite these, Univ. des Sci. et Tech., de Lille, 1995, p. 245.

Shaw, G. E., *Sun Photometry*, Bull. Am. Meterol. Soc. **64** (1983), 4–9.

Shettle, E. P. and R. W. Fenn, *Models for the Aerosols of the Lower Atmosphere and the Effects of Humidity Variations on Their Optical Properties*, Report AFGL-TR-79-0214, Air Force Geophysics Laboratory, Hanscomb AFB, MA 01731, 1979.

Vigroux, E., *Contribution a l'etude experimentale de l'absorption de l'Ozone*, Ann. Phys. Paris **8** (1953), 709–762.

Voss, K. J., *Electro-optic Camera System for Measurement of the Underwater Radiance Distribution*, Optical Engineering **28** (1989), 241–247.

——— and A. C. Chapin, *Next generationin-water radiance distribution camera system, Society of Photo-OpticalInstrumentation Engineers*, Ocean Optics 11 **1750** (1992), 384–387.

——— and G. Zibordi, *Radiometric and Geometric Galibration of a Visible Spectral ElectroOptic "Fisheye" Camera Radiance Distribution System*, Jour. Atmos. and Oceanic Technology **6** (1989), 652–662.

Wang, M. and H. R. Gordon, *Retrieval of the Columnar Aerosol Phase Function and Single Scattering Albedo from Sky Radiance over the Ocean: Simulations*, Applied Optics **32** (1993), 4598–4609.
Young, A. T., *Revised depolarization corrections for atmospheric extinction*, Applied Optics **19** (1980), 3427–3428.

Figure Captions

Figure 1a. An example of downwelling irradiance, upwelling radiance, and downwelling irradiance above the sea surface measured with the MOS.

Figure 1b. Spectra of the downwelling irradiance attenuation coefficient (Ke), the upwelling radiance attenuation coefficient (Kl), and the water-leaving radiance derived from the data in Figure 1a.

Figure 2a. An example of three langley regressions at different wavelengths to obtain the total optical depth. The slope of this line is directly the total optical depth, while the intercept is the calibration constant for the instrument. These measurements were obtained on the Mauna Wave during November 1994 (MOCE-3)

Figure 2b. The variation of optical depth with wavelength for the data set shown in Figure 2a. The total optical depth is measured via the langley regressions, Rayleigh optical depth is calculated, and the ozone optical depth is derived from ozone climatologies and ozone absorption coefficients as described in the text. The Aerosol optical depth is the residual after the Rayleigh and ozone optical depths are subtracted from the total optical depth.

Figure 3. Contours of the sky radiance. Units for the contours are 10^{-2} μW/cm^2/sr/nm. Each plot corresponds to a different wavelength: A is 440 nm, B is 560 nm, C is 670 nm, and D is 860 nm. The large object in the lower left of each image is the occulter which blocks the direct sunlight from hitting the lens surface. The zenith angle of the sun is 52°, and is obvious in images A, B, and C as bright spots on the occulter. In these plots the zenith angle is linearly related to the distance from the center of the image, with the edge of the image being approximately 85°. These images were obtained on the R/V Mauna Wave during October 1995.

Figure 4. Example of a map of the aerial distribution of phytoplankton pigments.

Figure 5. Schematic of the Marine Optical Buoy System (MOBY II).

Figure 6. Chart of the calibration/validation site occupied by MOBY, along with isopleths of mean wind speed in the vicinity of the site. Also shown are the ASSR site and the MobilNet relay sites.

Figure 7. Photograph of the deployed ASSR.

Table 1. Marine Optical Instrument and Buoy System Features

- Optical System
  - Dual Spectrographs
    - Dichroic Beam Splitter
    - Reflected 380-600 nm
    - Transmitted 630-900 nm
    - Holographic Gratings - Convex Being Tested
    - Flat Field
    - #1 Range 350-650 nm Blazed at 440 nm
    - #2 Range 600-900 nm Blazed at 700 nm
  - Linear Array Detectors
    - 512 Element Silicon Photodiode
    - 512 X 512 CCD Array Being Tested
    - Thermoelectric Coolers
  - Spectral Resolution
    - 1 nm for Array Calibration
    - 3-4 nm In-situ Observations
  - Collectors
    - Vector Irradiance
    - Telescopes - Radiance
    - Fiberoptic Mutiplexer-Ten Remote Collectors
  - Calibration
    - Two Internal LED References (blue-green & red)
    - Quartz Halogen Reference Lamp
    - Erbium Doped Spectralon (Labsphere)
- Ancillary
  - Pressure
  - Temperatures (water, instrument housing , detectors)
  - Magnetic Heading
  - Inclination (two-axis)
- Data Acquisition
  - Direct Serial Link (9600 baud)
  - Telemetry (ARGOS)
  - Cellular Telephone
- Data Acquisition Software
  - DEC/VMS & MS/DOS
- Data Reduction & Analysis Software
  - DEC/VMS
  - MS/DOS
- Deployment
  - Ship
  - Moored Buoys
- Satellite Positioning
  - Global Positioning System
  - Argos
- Data Archive
  - Near-real time & historical
  - Internet Access

MODIS Marine Optical Characterization Experiment 3

CRUISE: MOCE-3 SHIP: R/V Moana Wave
STATION: 4 - Kauna Point

Top = 1 m (solid)
Mid = 6 m (dashed)
Bot = 21 m (dotted)

POSITION: 19 08.4 N 155 55.9 W
DATE: 23:53 (GMT) 01 Nov 1994

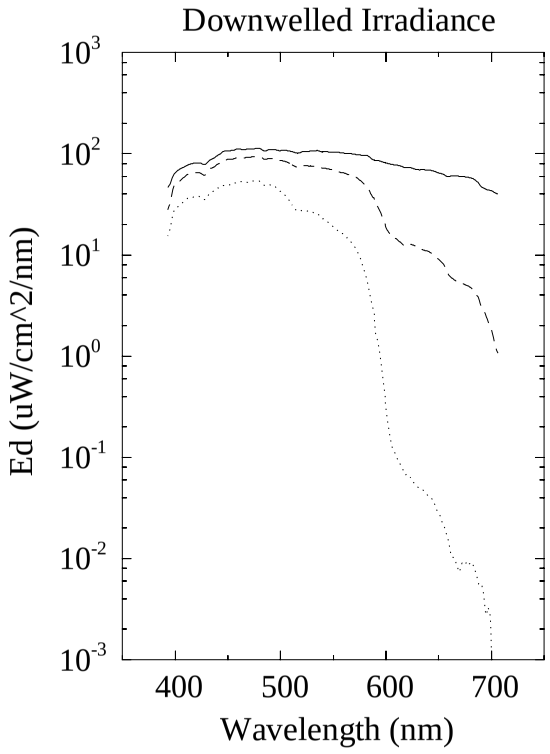

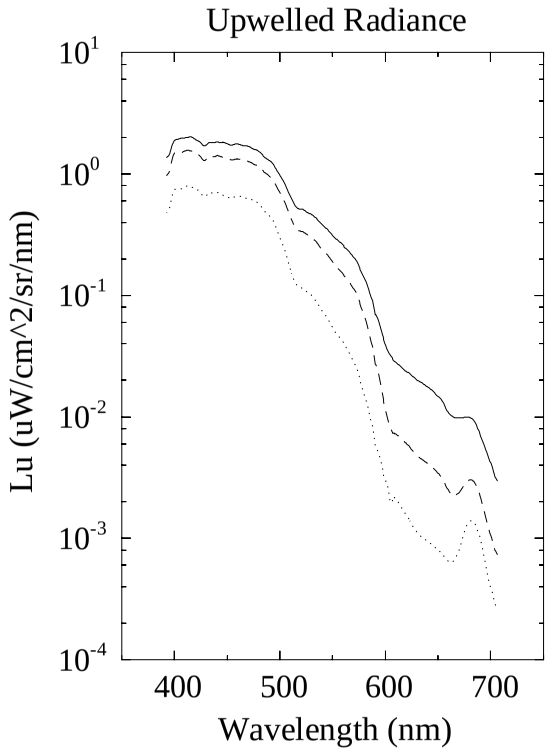

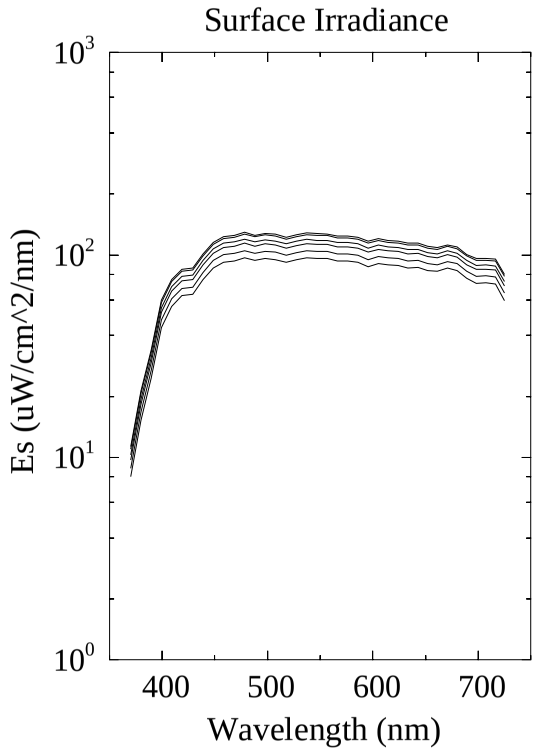

MODIS Marine Optical Characterization Experiment 3

CRUISE: MOCE-3 SHIP: R/V Moana Wave
STATION: 4 - Kauna Point

Top = 1 to 6 m (solid)
Mid = 1 to 21 m (dashed)
Bot = 6 to 21 m (dotted)

POSITION: 19 08.4 N 155 55.9 W
DATE: 23:53 (GMT) 01 Nov 1994

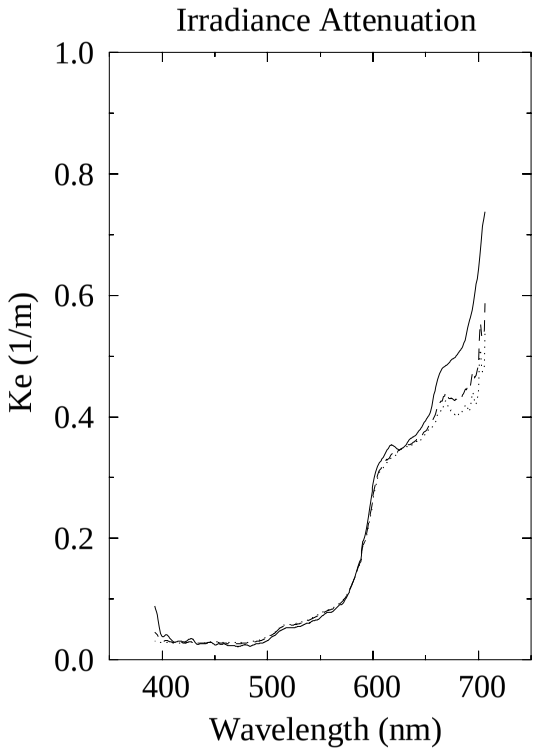

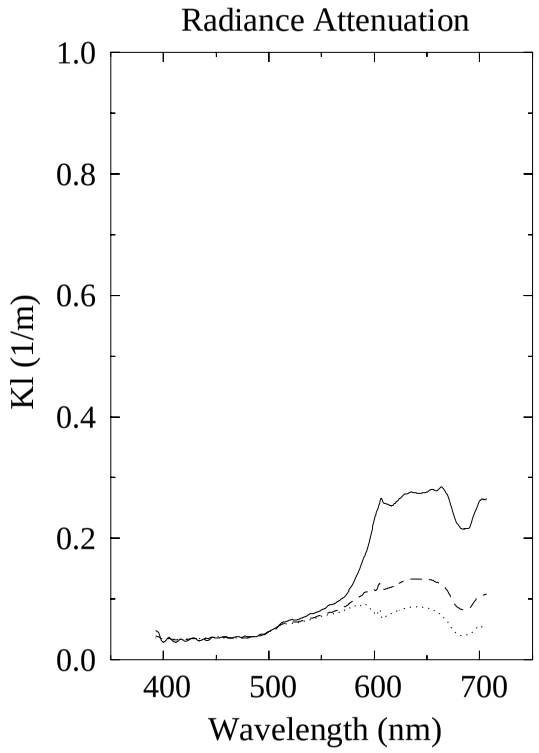

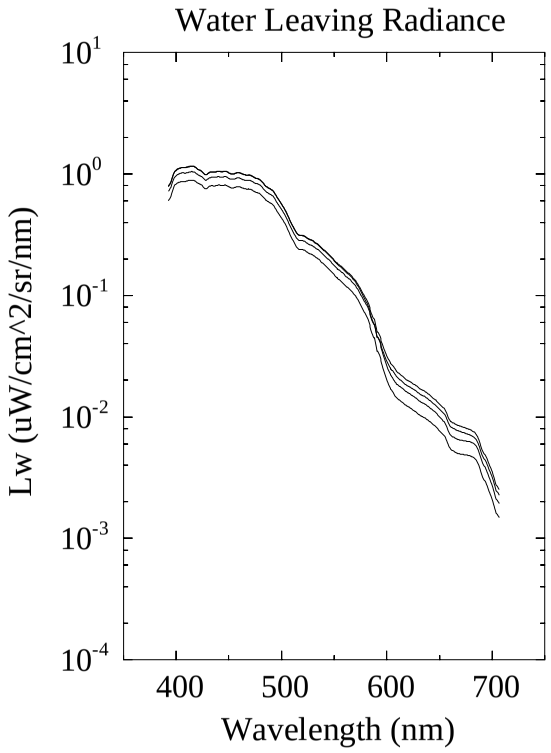

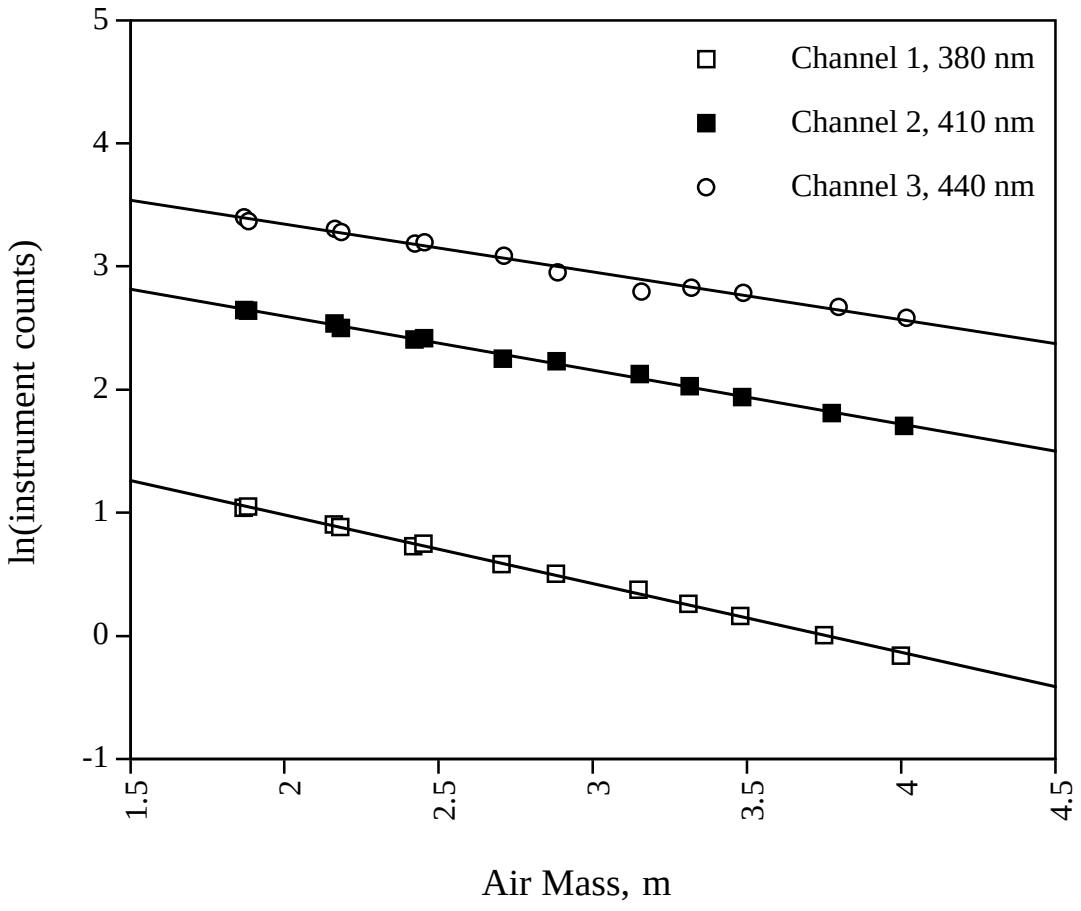
Channel 1, 380 nm
Channel 2, 410 nm
Channel 3, 440 nm
ln(instrument counts)
Air Mass, m
5
4
3
2
1
0
-1
1.5
2
2.5
3
3.5
4
4.5

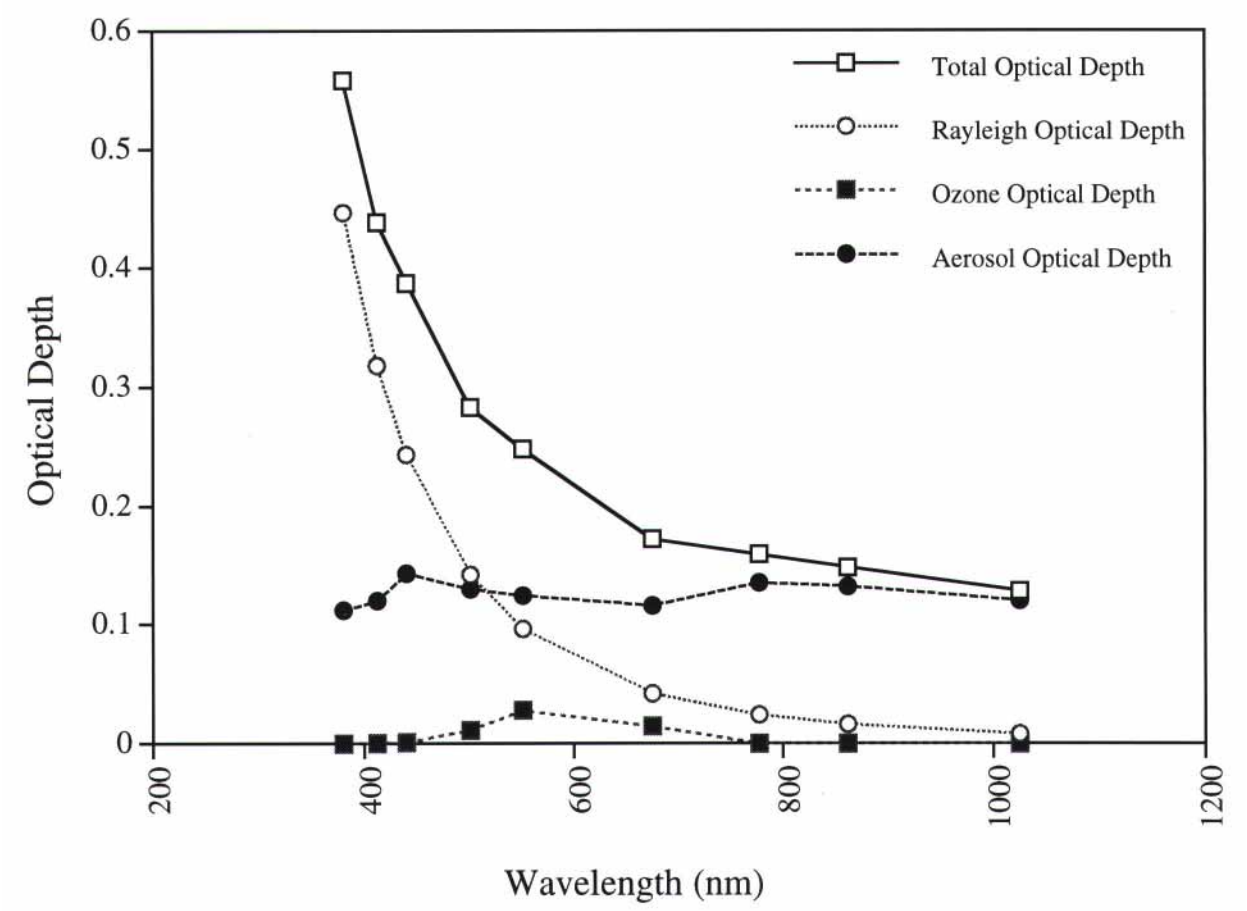
Optical Depth
0.6
0.5
0.4
0.3
0.2
0.1
0
200
400
600
800
1000
1200
Wavelength (nm)
Total Optical Depth
Rayleigh Optical Depth
Ozone Optical Depth
Aerosol Optical Depth

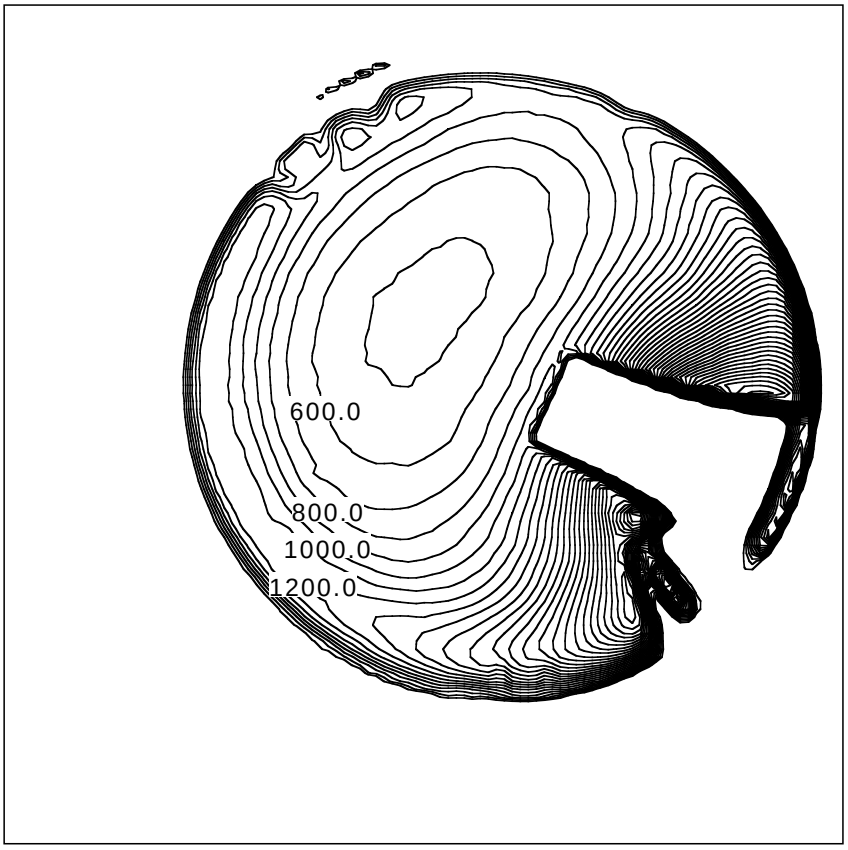
600.0
800.0
1000.0
1200.0

B

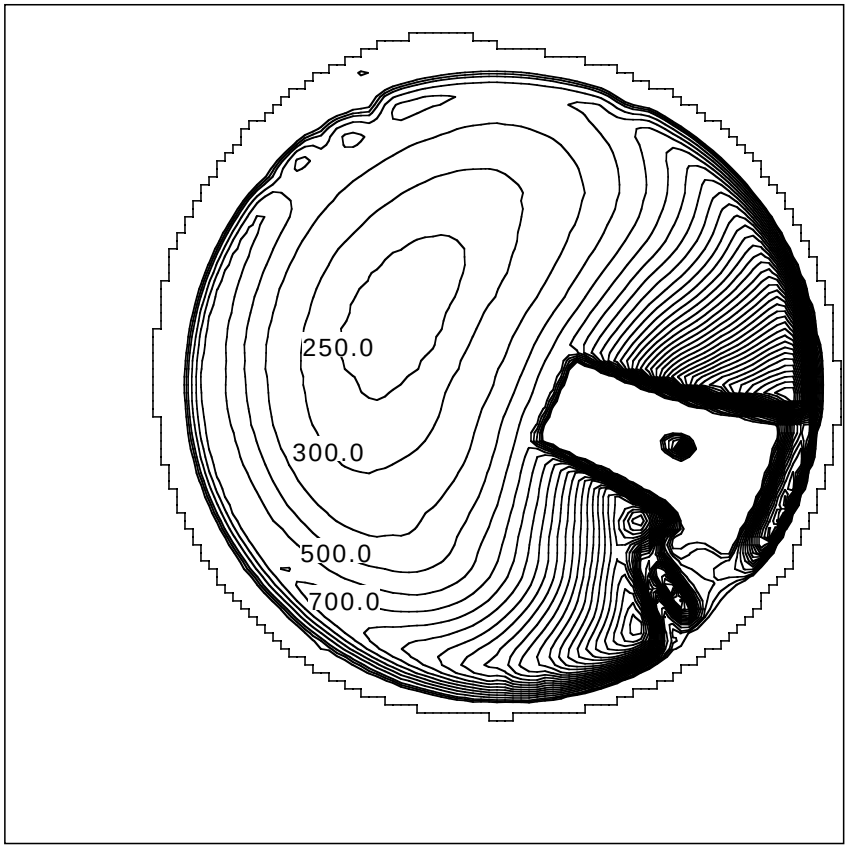

C

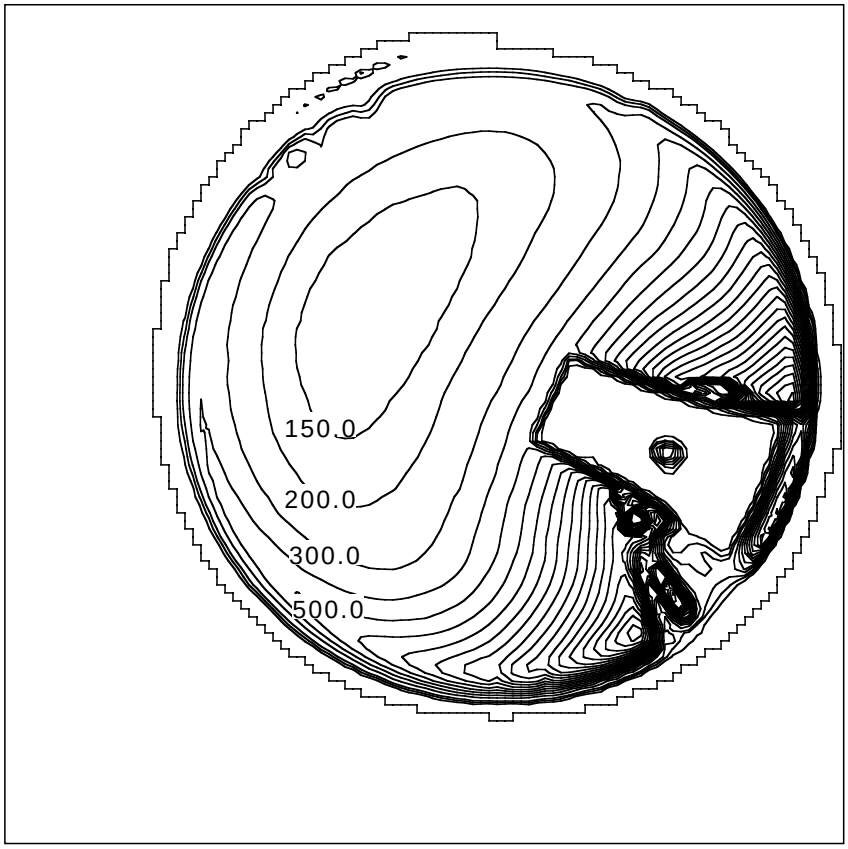

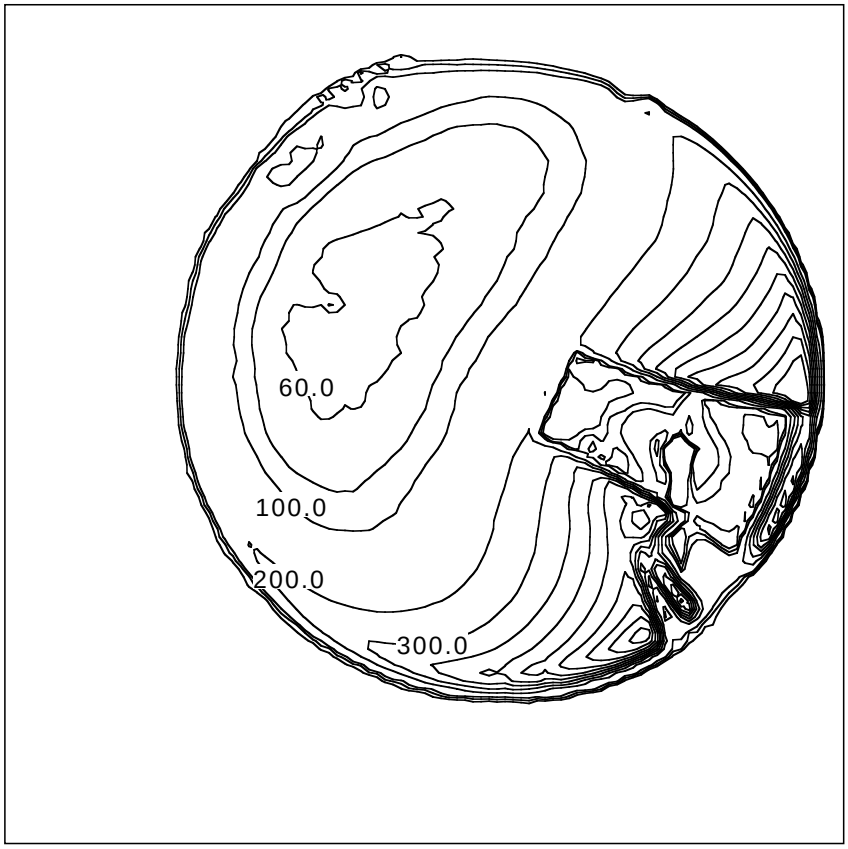
60.0
100.0
200.0
300.0

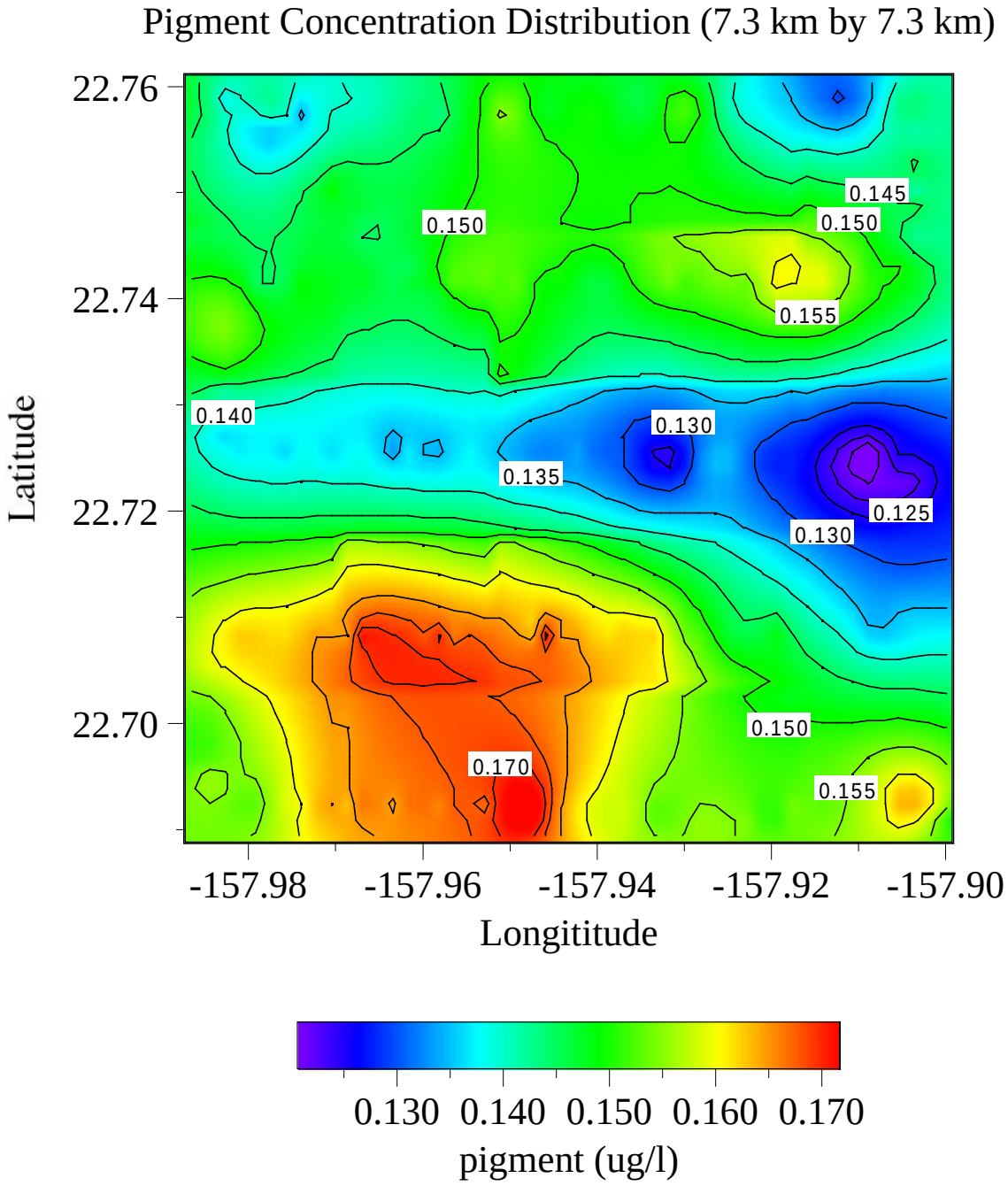

pigment_ug_l vs. (row, col)

MOBY

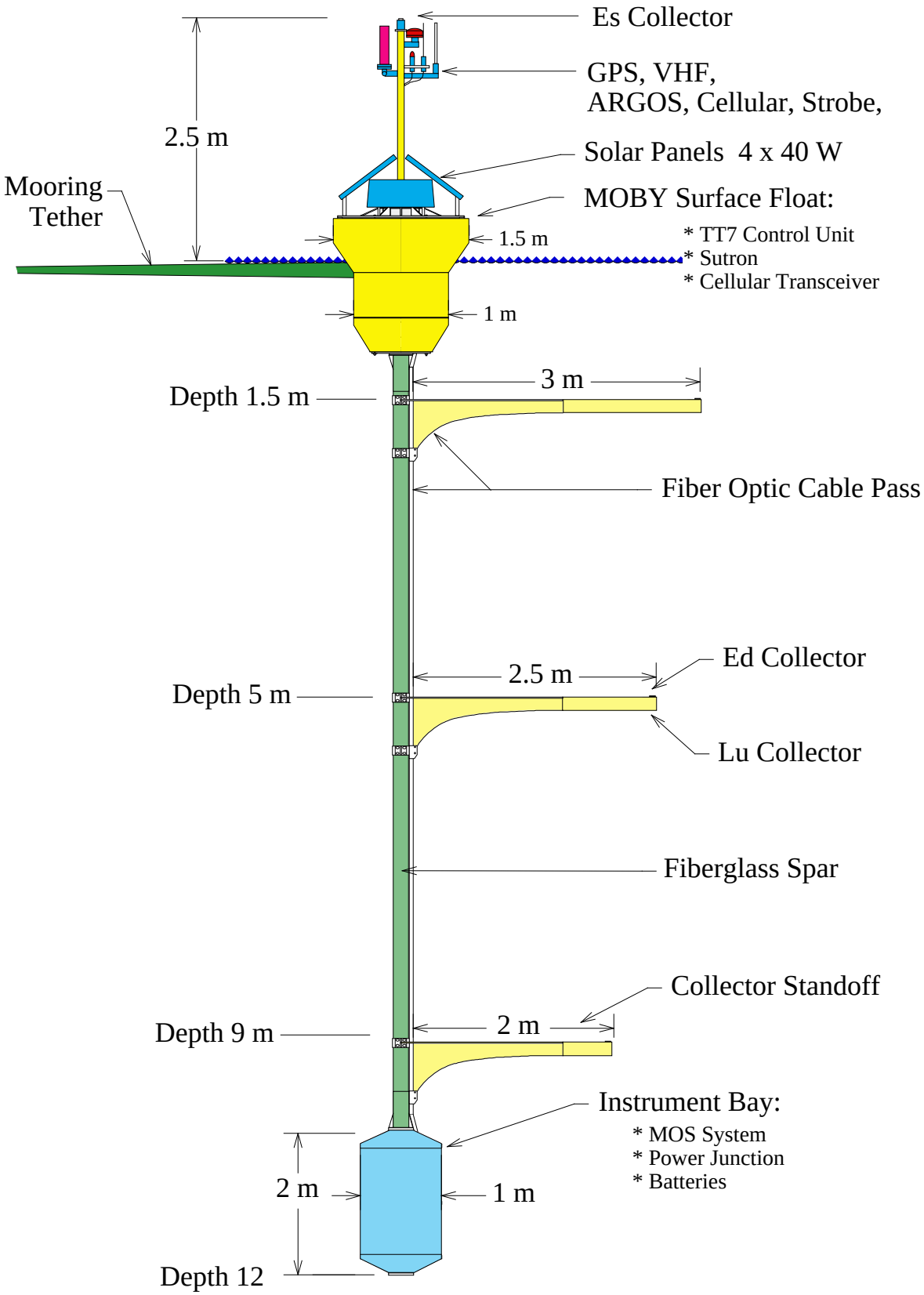
Es Collector
GPS, VHF,
ARGOS, Cellular, Strobe,
Solar Panels 4 x 40 W
MOBY Surface Float:
* TT7 Control Unit
* Sutron
* Cellular Transceiver
2.5 m
Mooring
Tether
1.5 m
1 m
Depth 1.5 m
3 m
Fiber Optic Cable Pass
Depth 5 m
2.5 m
Ed Collector
Lu Collector
Fiberglass Spar
Collector Standoff
Depth 9 m
2 m
Instrument Bay:
* MOS System
* Power Junction
* Batteries
2 m
1 m
Depth 12

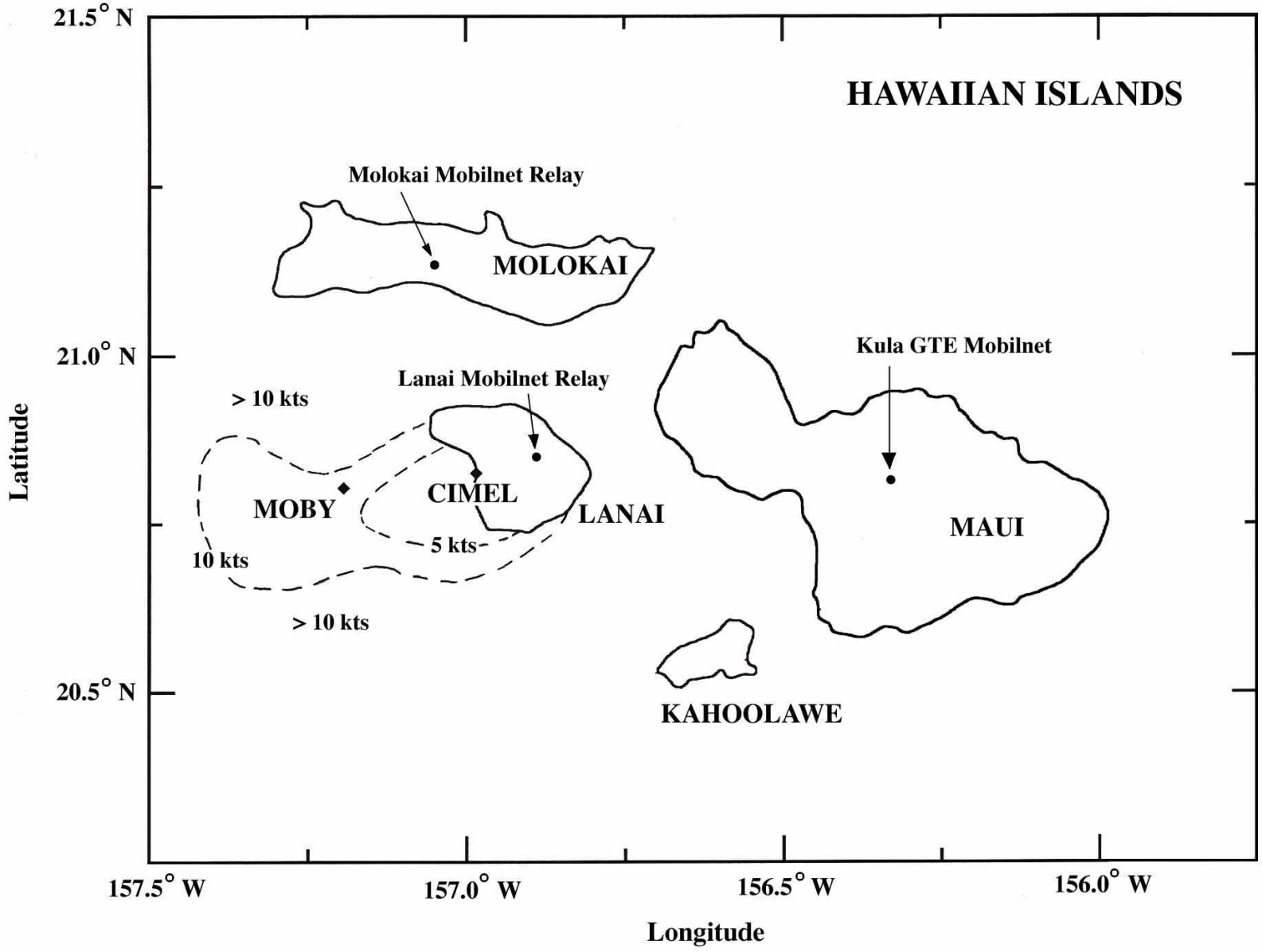
HAWAIIAN ISLANDS
Molokai Mobilnet Relay
MOLOKAI
Kula GTE Mobilnet
Lanai Mobilnet Relay
> 10 kts
MOBY
CIMEL
LANAI
MAUI
5 kts
10 kts
> 10 kts
KAHOOLAWE
21.5° N
21.0° N
20.5° N
Latitude
157.5° W
157.0° W
156.5° W
156.0° W
Longitude